2022-12-01

Sulfonated Styrene Grafted SEBS/ABS Made by Additive Manufacturing for Ion Exchange Applications

Avianna Elaine Gallegos
University of Texas at El Paso

SULFONATED STYRENE GRAFTED SEBS/ABS MADE BY ADDITIVE MANUFACTURING FOR ION EXCHANGE APPLICATIONS

AVIANNA ELAINE GALLEGOS

Master's Program in Civil Engineering

APPROVED:

William Shane Walker, Ph.D., Chair

Eva Deemer, Ph.D., Co-Chair

David Roberson, Ph.D.

Ivonne Santiago, Ph.D.

Malynda Cappelle, Ph.D.

Stephen L. Crites, Jr., Ph.D.
Dean of the Graduate School

SULFONATED STYRENE GRAFTED SEBS/ABS MADE BY ADDITIVE MANUFACTURING FOR ION EXCHANGE APPLICATIONS

by

AVIANNA E. GALLEGOS, B.S.

THESIS

Presented to the Faculty of the Graduate School of

The University of Texas at El Paso

in Partial Fulfillment

of the Requirements

for the Degree of

MASTER OF SCIENCE

Department of Civil Engineering

THE UNIVERSITY OF TEXAS AT EL PASO

December 2022

Acknowledgements

Thank you to Dr. Shane Walker, Dr. Eva Deemer, and Joe Feuille for making the completion of this paper possible with your extensive help at every step. Thank you to my other committee members, Dr. Malynda Cappelle, Dr. David Roberson, and Dr. Ivonne Santiago, for accommodating your busy schedules to lend your expertise to this research. Moreover, thank you to Dr. David Roberson and Truman Word at the UTEP Polymer Extrusion Lab and Dr. Leo Banuelos at the UTEP Physics Department for your collaboration.

Thank you to my peers at the Center for Inland Desalination Systems, and thank you to the Nanosystems Engineering Research Center for Nanotechnology Enabled Water Treatment for partially sponsoring this research.

Lastly, I will never be able to express how grateful I am for my amazing family, whose place in my life means everything.

Abstract

An interpenetrating polymer network (IPN) for cation exchange applications was synthesized from a blend of styrene-ethylene/butylene-styrene (SEBS) and acrylonitrile butadiene styrene (ABS), which was 3D printed, grafted with crosslinked polystyrene (PS), and sulfonated. A method for styrene grafting was applied to reduce the damage to polymer phases caused by the sulfonation reaction. Styrene and divinylbenzene monomers were introduced to the IPN and induced with heat treatment to polymerize *in situ.* The graft copolymerization reaction was enhanced with varying quantities of benzoyl peroxide as a chemical initiator. The samples were subsequently sulfonated with chlorosulfonic acid in dichloroethane and functionalized for ion exchange. These samples' chemical composition and morphology were characterized by the ion exchange capacity (IEC), FTIR spectroscopy, SEM imaging, and small angle X-ray scattering (SAXS). Analysis of the samples revealed that higher quantities of benzoyl peroxide improved the degree of grafting and created a more highly ordered internal arrangement of the styrene domains in the network. As a result, the resistance of ABS to chemical solvents was significantly improved, and the integrity of the polymer domains was protected from the sulfonation reaction. Lastly, the methodology was improved with respect to the swelling agent used in the sulfonation reaction. Samples were sulfonated with chlorosulfonic acid in dichloroethane, dichloromethane, and chloroform. Dichloroethane appeared to have the least destructive effect on the integrity and linearity of the polymer blend. These results indicate that a methodology and chemistry for producing ion exchange material from blended and 3D-printed SEBS/ABS polymers were successfully developed. This new strategy for functionalizing polymer blends can be applied in the future to improve the mechanical stability of membranes without the need for chemical crosslinking.

Table of Contents

List of Figures

Chapter 1: Introduction

The water-energy nexus approach has become increasingly relevant as population growth and changing population patterns exacerbate the scarcity of these two resources around the world (Dai et al., 2018; Hamiche, Stambouli, & Flazi, 2016). The nexus approach highlights the need to manage efficient energy consumption and clean water availability as mutually dependent demands. Advancements of renewable energy sources account for higher percentages of the global energy budget, but their often-intermittent availability and lack of intrinsic storage capabilities prompt the need for simultaneous advancements in efficient and large-scale energy storage systems. More fundamentally, proper drinking water and wastewater treatment is an essential limiting factor to human health, environmental protection, and many modern industrial/commercial activities. Only 2.5% of all water on Earth is freshwater, most of which is frozen in ice sheets and glaciers (Igor A. Shiklomanov, 1993).

Consequently, a primary goal of the water resource sector is to mobilize the availability of brine and brackish water as viable drinking sources by efficiently removing the maximum possible concentrations of minerals and pollutants (Lee, Elam, & Darling, 2016). Additionally, a progressive approach to wastewater treatment seeks not only the removal of harmful chemicals and toxic substances but an intensified focus on resource recovery of valuable metals and nutrients (Zuo, Wang, DuChanois, et al., 2021). These applications — water reuse & treatment, wastewater recovery, large-scale energy storage, and commercial/industrial manufacturing — share a common need for materials' separation, concentration, and purification. Membrane separation processes are a competitive alternative to conventional chemical treatment, physical separation, and thermal desalination techniques. They separate constituents by selective filtration across an engineered

semi-permeable material and have gained an established reputation in practical applications (Strathmann, 1981).

Ion exchange materials (IEMs) separate ionic constituents as they travel through the channels of the material's porous matrix. The channels carry fixed functional groups which imbue the IEM with an overall fixed positive or negative charge. This charge facilitates a chemical interaction in which oppositely charged ions from a contacting electrolyte solution are electrochemically attracted to the fixed-charged sites and allowed to travel through the pores. Meanwhile, ions of the same charge as the IEM are prevented from traveling through the channels due to the Donnan exclusion effect. The ions that can travel through the nanochannels, referred to as mobile counterions, become loosely incorporated into the matrix by electrostatic attraction to the fixed charged sites. (Dahman, 2017). Because these counterions are mobile and not permanently attached to the matrix, they can be displaced by other species of incoming counterions. This opportunity for displacement facilitates an exchange of ions, as the original species is replaced by the incoming species and forced to travel back out of the matrix. In membrane separation processes, this exchange phenomenon is used to strategically remove targeted ionic species from a contacting solution and separate them out through the membrane barrier.

1.1 Ion Exchange Materials

Membrane separation technology is competitive in performance and cost thanks to recent advancements in the material sciences (Zuo, Wang, DuChanois, et al., 2021). The sulfonated perfluorinated polymer electrolyte membrane Nafion was the first synthetic ionomer of its kind, and its properties for ion exchange applications have been widely studied. Nafion is a

polytetrafluoroethylene (PTFE) material; the tetrafluoroethylene in Nafion forms a hydrophobic backbone, while the sulfonyl fluoride vinyl ether side chains self-organize into hydrophilic functional clusters that work to draw water from the environment (Stenina, Golubenko, & Nikonenko, 2020). As a result of the self-organized hydrophilic-hydrophobic clusters, a network of channel-like pores form in the polymeric membrane and allow for the selective transport of ionic constituents through the electrically conductive matrix (Stenina et al., 2020). Despite its excellent chemical stability and high conductivity, Nafion is expensive to produce, and the environmental/human health concerns surrounding the use of PFAS (Per- and polyfluoroalkyl substances, AKA. "Forever chemicals") are well-documented (H. S. Park & Hong, 2021; Conley, 2019)).

On the other hand, membranes made of a hydrocarbon base and functionalized with polar groups to mimic the hydrophobic-hydrophilic combo of PFTE are comparatively less expensive and detrimental to the environment (Müller et al., 2012). Though they have shorter usable lifespans than fluorinated polymers, they can be enhanced with various modifications to achieve chemical stability, thermal resilience, and transport properties comparable to those of PFTE materials. Neosepta, Fumatech, and Fujifilm fabricate commercial hydrocarbon IEMs with pseudo-homogeneous morphologies (Stenina et al., 2020).

In the last few years, 3D printing has entered the water treatment scene, opening the door to a new method of manufacturing separating membranes. While traditional techniques for synthesizing membranes, such as solvent casting, are being criticized for using environmentally detrimental chemicals, additive manufacturing avoids some drawbacks while being more scalable, versatile, and cost-effective. Although the resolution capabilities of current 3D printing methods are still a long way from direct membrane fabrication, efforts to incorporate additive

manufacturing into various components of water desalination technology have grown in the last five years (Khalil, Ahmed, & Hilal, 2021).

Many papers have been published on optimizing IEMs made of monomers and blended copolymers. However, research still seeks to improve the dimensional stability, operating temperature resistance, and selectivity vs. permeability limits of these polymers when functionalized for ion exchange (Scott & Hughes, 1996). A popular candidate for addressing some of these improvements is polystyrene-block-poly-(ethylene-ran-butylene)-block-polystyrene (SEBS), a triblock copolymer that is abundant, thermochemically resilient, and readily modifiable for electroactive properties (Yu, Dong, Li, Wang, & Yang, 2021). For these reasons, it has attracted attention as a promising starting material for ion exchange membranes. The styrene aromatic rings in the SEBS chain provide locations where functional groups can attach. Because the copolymer is very phase-segregated between the polystyrene and ethylene-butylene blocks, functionalization results in excellent microphase separation between the strongly hydrophobic backbone and well-incorporated hydrophilic functional clusters (Mokrini & Huneault, 2006). This self-assembling separation creates defined and organized channels to support ionic transport through the material. In this paper, we were interested in maximizing the sulfonation potential of a SEBS base for ion exchange by increasing the styrene rings in the polymer chain. To do this, SEBS was used as the membrane support, and additional styrene monomers were grafted to the polymer chain (Sherazi, 2016).

The pursuit of achieving the highest ion exchange capacity while maintaining proper mechanical stability has dominated the discussion on membrane synthesis. However, surface morphology is a significant and underestimated component in the actual functionality of membranes for ion exchange applications. In proton exchange membranes, the sulfonation

reaction not only polarizes the membrane by incorporating negatively charged sulfone groups into the polymeric matrix but also has the potential to enhance the membrane's water transport properties and resistance to fouling if the conditions of the reaction proceed in a manner that enhances desirable morphology (Zuo, Wang, Duchanois, et al., 2021). The morphology of the membranes — nanochannel uniformity and organization of functional domains — is primarily dictated by the phase separation that occurs during the functionalization reaction (Orujalipoor et al., 2019). Polymers can be sulfonated either by direct copolymerization or post-sulfonation methods (H. S. Park & Hong, 2021). In the sulfonation reaction, the sulfonating agent, reaction time, and temperature can be optimized to achieve desired electrochemical properties and surface morphology.

The simplest way to synthesize an ion exchange material with high conductivity is by increasing the number of fixed ionic groups in the matrix via intensified sulfonation. However, a higher degree of sulfonation compromises the mechanical integrity of the material and leads to excessive swelling. A more sophisticated way to facilitate transport/ion mobility is to control and achieve highly ordered and separated phase morphology. Marked phase separation achieves interconnected channels while maintaining a limited ion exchange capacity value, as in the highly interconnected and microphase-separated Nafion morphology. For example, Wei et al. achieved desirable ion cluster sizes and distinct phase separation by introducing unfunctionalized hydrophobic side chains to the membrane (Wei et al., 2019). Similarly, Orujalipoor et al. published findings on structural shapes and distributions of the nanoaggregates in the polymeric matrix of SEBS (Orujalipoor et al., 2019). They concluded that longer sulfonation times were associated with smaller, more globular, and less orderly tunnels and smaller interplanar distances between the tubular aggregations.

In the sulfonation reaction, commonly used sulfonating agents for post-sulfonation methods include fuming sulfuric acid and chlorosulfonic acid (Barton, Patton, Hukkanen, & Bernius, 2017). Post-sulfonation with concentrated sulfuric acid is attractive because it is relatively inexpensive and plays the simultaneous role of sulfonating agent and solvent (Tavangar, Zokaee Ashtiani, & Karimi, 2020). On the other hand, it is aggressive and can cause damage to the morphology of resin beads and polymeric membranes (De Oliveira, De Aguiar, De Aguiar, & De Santa Maria, 2005). Post-sulfonation with chlorosulfonic acid in a halogenated solvent is less degrading to the polymer chain, but the use of solvent compromises the homogeneity of the sulfonated product (Iulianelli et al., 2010). Nagarale et al. previously explored the relationship between the solvent used in the sulfonation reaction and the electrochemical properties of the sulfonated product (Nagarale, Gohil, Shahi, & Rangarajan, 2005). However, the study did not look at the morphology of the membranes. In this paper, we were interested in observing any outstanding morphological effects that might render one sulfonation solvent more advantageous than another for ionic transport and overall resilience.

1.2 Goals and Objectives

This research aimed to quantify the effects of the chemical initiator in the success of the graft copolymerization reaction and determine if a favorable morphology could be observed for selecting one solvent over another in the sulfonation reaction for functionalization.

Our study achieved three objectives:

1. Grafted polystyrene to novelty 3D-printed interpenetrating polymer network (IPN) samples made of SEBS and ABS (acrylonitrile butadiene styrene) and sulfonated them for ion exchange applications.

2. Improved the degree of polystyrene grafting with higher concentrations of benzoyl peroxide as the chemical initiator.

3. Performed a comparative analysis of the effects on favorable morphology of the solvent used during the sulfonation reaction with chlorosulfonic acid.

A SEBS triblock copolymer and ABS blend were extruded, and 3D printed into membrane sheets. Styrene with a percentage of divinylbenzene crosslinker and variable amounts of benzoyl peroxide initiator was successfully grafted onto the membrane. The grafted SEBS-ABS/styrene membranes were sulfonated using the chlorosulfonic acid-in-solvent method. The membranes were sulfonated using three different solvents commonly used in literature and patents — dichloroethane (DCE), dichloromethane (DCM), and chloroform (CHL). The effects of variable amounts of initiator during grafting and the effects of different solvents during sulfonation on the ion exchange properties and the surface morphology of the membranes were determined via ion exchange capacity test, SEM imaging, FTIR elemental analysis, and Small Angle X-Ray Scanning.

Chapter 2: Literature Review

The organization of the literature review portion of this investigation has been summarized in Figure 2.1. A particular focus was placed on studying recent publications that employed multi-step methodologies for improving the properties of the polymer base before and through the sulfonation reaction.

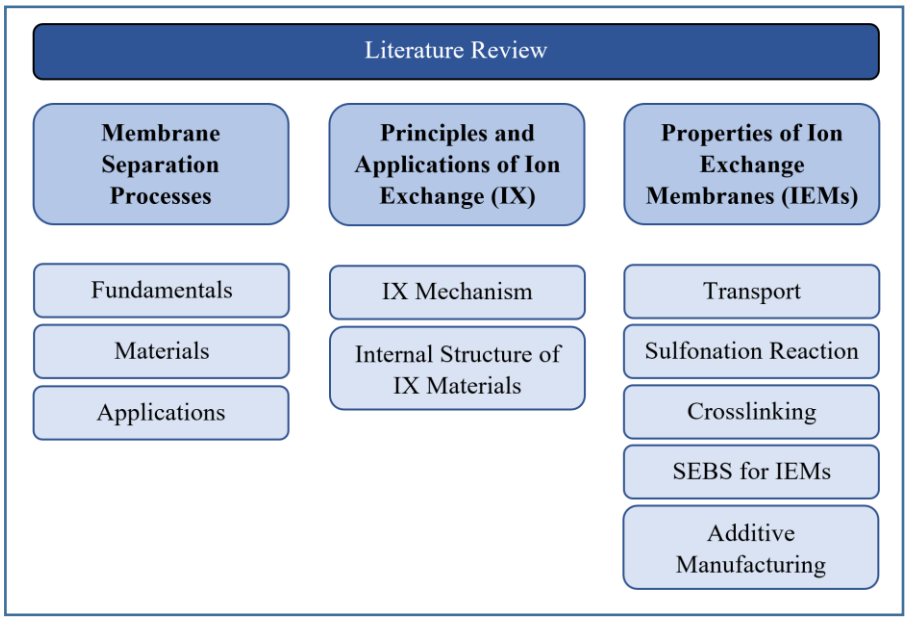

Figure 2.1 Overview of Literature Review chapter

2.1 Membrane Separation Processes

Membrane separation processes have become a competitive alternative to conventional chemical treatment, physical separation, and thermal desalination techniques. Thermal desalination processes, in which saline water is heated to vapor and subsequently condensed, have historically drawn criticism for their energy-intensive and costly nature. Although advancements in thermal desalination by using renewable energy sources show great promise, developments are still largely confined to the laboratory research phase (Gude, 2018; Kondili, 2012). By contrast, membrane processes operate on the principle of separating constituents by selective filtration across an engineered semi-permeable material and have gained an established reputation in

practical applications (Strathmann, 1981). Advanced selective membrane processes are versatile, efficient, methodized, and have relatively low energy consumption. The membranes are compact and modular in design and have highly customizable properties made possible by rapid innovations in material science research (Zuo, Wang, DuChanois, et al., 2021). Due to their performance and cost advantages, their implementation extends widely to water and wastewater treatment & resource recovery (Zuo, Wang, DuChanois, et al., 2021), pharmaceutical production (Sirkar, 2000), food processing (Guiga & Lameloise, 2019), and fuel cells (Zaidi & Matsuura, 2009).

The membrane uses the effects of concentration gradient, temperature, pressure application, or electric potential to facilitate the controlled transport of a particular species through itself; this controlled separation across the membrane barrier produces a stream depleted of the species on one side and another stream concentrated with it on the other (Scott & Hughes, 1996). This technique can separate mixtures, dispersions, and solutions in phases. Membranes are broadly characterized by fundamental properties such as permeating phase, porosity, symmetry, homogeneity, electrochemical charge, and transportation mechanism (Prifti, Parasuraman, Winardi, Lim, & Skyllas-Kazacos, 2012).

Commercial membranes can be made of a wide variety of organic and inorganic materials; synthetic polymers are most widely studied and used because they are economical, adaptable, and scalable for manufacturing (Zeman & Zydney, 2017). Common examples of these polymers include modified cellulose, polysulfones, polyamides, and perfluoro polymers (Lee et al., 2016). These materials are carefully designed and optimized to maximize the membrane's chemical resistance, thermal stability, mechanical framework, permeability, and selectivity (Scott & Hughes, 1996). A common design tradeoff is that, although thinner membranes are more

permeable (and thus more efficient), their mechanical stability and selectivity are reduced (L. Y. Jiang, 2016).

Pressure-driven membrane separation processes include microfiltration (MF), ultrafiltration (UF), nanofiltration (NF), and reverse osmosis (RO). In MF and UF, a pressure gradient applied across a porous membrane drives the separation of particulates by size exclusion through simple sieving action. In 1964, Loeb and Sourirajan published a new method to produce asymmetric membranes with a thin yet dense active "skin" layer over a thick and porous support layer made from the same material (Patent No. 3,133,132, 1964). These novel membranes exhibited higher flux with better mechanical integrity at a reduced cost (Strathmann, 1986). This development and the subsequent branching into composite membranes revolutionized the membrane technology field and enabled reverse osmosis to become a viable method for water desalination (Qian et al., 2022). Reverse osmosis and nanofiltration separate ions by size and chemical exclusion (Berk, 2009). The solution-diffusion model explains the transport of ionic constituents through an RO membrane, in which separation occurs due to variable rates at which different permeants dissolve and diffuse across the membrane (S. Kim, 2021; Wijmans & Baker, 1995).

Other membrane processes include dialysis (de Castro, Capote, & Ávila, 2008), gas separation (Bernardo, Drioli, & Golemme, 2009), electro-osmosis (Pretorius, Hopkins, & Schieke, 1974), pervaporation (Kumar Purkait, Singh, Mondal, & Haldar, 2020), thermo-pervaporation (Sanchez Fernandez, Geerdink, & Goetheer, 2010), membrane distillation (Alkhudhiri & Hilal, 2018), and electrodialysis (Xu & Huang, 2008). Electrodialysis, which selectively separates ions of opposite charges, is part of a broader category of membrane separation that operates by ion exchange.

Ion exchange membranes (IEMs) are distinguished from other inert membranes by the permanent electric charge embedded in the polymeric matrix, which enables the electro-driven separation of charged ionic constituents. IEMs are most broadly characterized as cation or anion exchange membranes. Cation exchange materials are permeable to positively charged cations and impermeable to negatively charged anions. The degree to which anions are excluded determines the performance of the IEM; the principle is inverted in anion exchange materials. The widespread applications and unique material principles of ion exchangers have become a popular focus of membrane separation research.

2.2 Principles and Applications of Ion Exchange

Ion exchange materials (IEMs) separate ionic constituents in an electrolyte solution by carrying a fixed positive or negative charge in their backbone, which repels similarly charged ions and attracts oppositely charged ions. The fixed charge is obtained when a porous, insoluble material is reacted with a functional ionogenic (or polar) group. In this functionalization reaction, the polar groups attach to locations throughout the material's internal structure; these attachment points become active sites that give the material an overall positive or negative charge. If the IEM acquires a negative charge with functional groups such as $-SO_3^-$, $-COO^-$, or PO_3^{2}-, it repels negative and attracts positive ionic constituents by Coulomb force and becomes a cation exchange material (CEM). If the IEM acquires a positive charge with functional groups such as $-NH_3^+$, $NH_2^{+,}$ or N^+, it repels positive and attracts negative ionic constituents by Coulomb force and becomes an anion exchange material (AEM). (Helfferich, 1922)

Both types of IEMs — anion exchange and cation exchange — have many uses. For example, ions are separated in electrodialysis by stacking CEM and AEM membranes and

applying an electric current through the stack. The alternating membranes selectively restrict or facilitate the movement of different ionized constituents in a contacting solution, such that the system produces separate streams of concentrated electrolyte and ion-free (relatively ion-free, since IEMs are never 100% selective) diluate (Garg, 2019). Electrodialysis has many applications in the concentration, removal, and recovery of ionic constituents, although the most extensive uses are the desalination of seawater and the deionization of solutions. AEMs and CEMs have important uses on their own, as well. For example, cation exchange membranes are used in proton-exchange membrane (PEM) fuel cells, and cation exchange resins are used in columns for water deionization (Abrams & Millar, 1997; Das, Choi, Nguyen, Kim, & Yoon, 2022).

The absorbance of dissolved species through an ion exchanger requires contact between an aqueous medium and an ionized exchange material (Scott & Hughes, 1996). The ions in the aqueous medium repelled by the IEM (due to having the same charge as the IEM) are called co-ions; the ions attracted to the IEM (due to having the opposite charge as the IEM) are called *counterions*. When these counterions enter the transportation channels of the matrix, they travel through as they are drawn to the active sites created by the functional groups. When they arrive at the active sites, the polar attraction between them and the ionized functional groups leads them to loosely bond, and the IEM system becomes electrostatically neutral (Dharmalingam, Kugarajah, & Elumalai, 2022). The system's need to recover electroneutrality after the charged functional groups are embedded is the force that drives ionic transportation through it. Because the fixed functional group is insoluble and the counterions that enter the structure are soluble, the exchanger exists in an ionized state. The ionized state means that other species of incoming counterions can easily displace the counterions (S. Kumar & Jain, 2013). This displacement of species, as mobile counterions are attracted and bonded to the fixed functional groups and then replaced by incoming

counterions, constitutes the ion exchange phenomenon. Like in sorption, ion exchange is a surface phenomenon, but unlike sorption, it occurs in stoichiometrically equivalent quantities of counterions (S. Kumar & Jain, 2013). (Stenina et al., 2020)

An ion exchanger comprises a hydrophobic polymer backbone and a hydrophilic terminal group that functionalizes the inert polymer (Scott & Hughes, 1996). The former endows the exchanger with mechanical stability, while the latter draws the aqueous external medium into the material's pores to initiate the exchange reaction (S. Jiang & Ladewig, 2017). The pores are a network of channels that are formed as a result of self-organized hydrophilic clusters (H. S. Park & Hong, 2021). The functional clusters on the pore walls draw contacting electrolyte solution into the center space of the pores and cause them to swell to a size of 4-5 nm (Stenina et al., 2020). When the pores are swollen with the ionized, electrically neutral contacting solution, the exchange is facilitated between the mobile counterionic portion of the dissociated functional groups and the like-charged ions in the solution. (Stenina et al., 2020). Zuo et al. referred to this as the "microstructure [gel/interstitial phase] model," where the polymer backbone/functional group combo acts as a gel to keep the like-charged co-ions out, and the free volume of the interstitial pore space facilitates the transport of oppositely charged counterions through the channel network (Zuo, Wang, DuChanois, et al., 2021).

As a basic example, water softeners remove hardness by treating water through a column of ion exchange material. A typical commercial ion exchange resin consists of a styrene-divinylbenzene copolymer backbone with negatively charged sulfone groups attached to the aromatic rings (Michaud, 2011). The sulfonate functional groups are strong and create a highly dissociated anion resin capable of readily exchanging mobile counterions. The resin is conditioned with a concentrated Na^+ (cationic) solution, and the functional groups uptake the sodium ions to

the degree which maintains proper electroneutrality (Vagliasindi, Belgiorno, & Napoli, 1998). When the treatment water passes through the resin column, Mg^{+2} and Ca^{+2} cations enter the channels of the resin matrix, and the species of cations in the exchanger are redistributed. The redistribution of counterions at the active sites is not purely statistical (Helfferich, 1922). Due to the phenomenon of competitive partitioning, the counterions are redistributed so that the ionic species most attractive to the functional groups are preferentially kept in the matrix, while the less attractive species are exchanged out of the IEM (Y. Kim & Lawler, 2011). Various parameters, including the valence, atomic number, and concentration, determine the preference or affinity for one ionic species over another (Chen, Wei, Hassanvand, Freeman, & Kentish, 2020). In the case of water softening, by conditioning the sulfonate groups in the resin with Na^{+} ions, which have a lower affinity than Mg^{+2} and Ca^{+2} ions, the resin readily displaces the former and uptakes the latter. This exchange produces an effluent rich in soft sodium ions and free of the undesired hardness ions.

2.3 Properties and Synthesis of Ion Exchange Membranes

When ion exchange materials are fabricated as membranes, the principles of application combine the electrochemical properties of ion exchange materials and the ability of membranes to act as a wall between two constituents (Helfferich, 1922). Ion exchange membranes are frequently used in dynamic processes where the ionized constituents can be transported through the membrane by applying an electric potential to the system . Here, the membrane structure is the selective barrier between different streams of concentrated ions. In the case of Nafion, the pendant sulfonic acid groups SO_3H strongly dissociate into $-SO_3^-$ anions; these are fixed on the pore walls, and H^+ cations distribute themselves in an electric double layer concentrated near the charged pore surface (P. Kumar, Bharti, Kumar, & Kundu, 2018). The double layer creates a potential between

the pore surface and the suspending liquid (Miller, 2011). Even without an external energy supply, dissolved ions can be separated through the membrane thanks to the Donnan Exclusion effect (Sarkar, SenGupta, & Prakash, 2010). The phase boundary potential caused by the non-uniform distribution of mobile ions prevents counterions from diffusing out of the membrane unless another species of counter ions is replacing them; thus, counterions are readily admitted, pass through easily, and create convection through the membrane in the direction of their transfer (Kral, Aplin, & Maier, 2021). Meanwhile, the Donnan potential prevents co-ions from entering and readily passing through the membrane barrier to prevent an accumulation of electric charge in the matrix (Helfferich, 1922). When the Donnan exclusion is less effective, co-ions pass through more easily, and the membrane becomes a less efficient selective barrier.

The effectiveness of proper co-ion exclusion leads to the discussion on the permeability-selectivity tradeoff. As the size of channels increases, the ion mobility and membrane conductivity increase. High membrane conductivity is desirable in most applications for efficient transport. Typically, this means that more hydrophilic functional domains, and correspondingly higher ion exchange capacity (IEC), improve membrane conductivity and ion permeability. However, high selectivity is also necessary to effectively separate ionic constituents. When the matrix becomes more hydrophilic, the interstitial space of the channels widens. As the channels swell with a higher volume of electrically neutral pore solution, the Donnan forces of the double electric layer are weakened. The weakening of the double electric layer leads to a higher transfer of undesirable co-ions and nonpolar molecules through the membrane barrier; consequently, the selectivity is lowered. Additionally, higher hydrophilicity and excessive water swelling compromise the polymeric matrix's mechanical integrity and chemical stability. (Stenina et al., 2020)

Research seeks to improve the permeability-selectivity tradeoff to produce highly selective and suitably conductive membranes (i.e., membranes with high ion exchange capacity and limited water uptake). In CEMs, higher ion exchange capacity is achieved with a higher degree of sulfonation. Generally, this means longer sulfonation times (S. Jiang & Ladewig, 2017). Jiang et al. found that IEC could be designed by modeling sulfonation time and controlling the mass ratio of the functional polymers (S. Jiang & Ladewig, 2017). However, another investigation showed that, while sulfur incorporation was directly related to sulfonation time, ion exchange capacity was optimized at 5 minutes of exposure (Orujalipoor et al., 2019). Additionally, this investigation characterized the nanostructures of their SEBS-based membranes with SAXS profiling and found that varying the sulfonation times significantly affected the mean distribution and ordered size of the channel domains. In another case, it was found that the particular sulfonating agent and reaction temperature significantly affected the morphology of ion exchange resin beads (De Oliveira et al., 2005). This study found that, even at the lowest temperature, sulfonation with Hydrosulfuric Acid (H_2SO_4) produced more morphologic defects than sulfonation with the milder action of Acetyl Sulfate in 1,2-Dichloroethane as a swelling agent. Still, other papers have reported positive results for using sulfuric acid over other agents in achieving high ion exchange capacity. While the sulfonation chemistry should be carefully considered for engineering strong ion exchange potential, the goal should also be to design for a balanced polymer matrix density and uniform surface morphology (Orujalipoor et al., 2019).

One way to increase the mechanical stability of an ion exchange polymer is by crosslinking the matrix. Crosslinking increases the ionomer's resistance to oxidation and physical strength (Michaud, 2011). Synthetic crosslinking agents such as divinylbenzene can be added during polymerization to induce crosslink bonds between polymer chains. Ionically crosslinked polymers

have flexible bonds, resulting in less brittle membranes and resins than covalently or uncrosslinked networks (H. S. Park & Hong, 2021). However, crosslinking can be costly and usually complicates the manufacturing method with extra steps (Stenina et al., 2020). Under operation, densely crosslinked materials may suffer from inadequately slow kinetics at lower temperatures (Michaud, 2011). More importantly, crosslinking consumes some of the sites available for functionalization, lowering the ion exchange capacity of the material. There are ways to mitigate the reduction of IEC when crosslinking, for example, by using a crosslinking agent that generates fixed charged sites at the crosslink bonds (Pandey, Goswami, Sen, Mazumder, & Childs, 2003). The methodology of this paper enhanced the physical properties of SEBS material by grafting crosslinked polymers to it. The microporous films were filled with a styrene-monomer/divinylbenzene-crosslinker mixture, and in-situ polymerization was initiated for successful grafting.

Styrene-Ethylene-Butylene-Styrene (SEBS) triblock copolymer is a promising material for membrane manufacturing because of the resilient and customizable properties that are characteristic of block copolymers (Seo et al., 2012). Compared to Nafion, its structure is simple: phase-separated hard and soft blocks are physically crosslinked by styrene domains that disappear when heated and reform when cooled (H. S. Park & Hong, 2021). As a result, it is extruded easily but deforms and shrinks unless blended with another thermoplastic. The nature of these crosslinks makes SEBS promising for applications in pervaporation and RO, and extra crosslinkers can be introduced to reduce water swelling for applications in electrodialysis, for example, when one study successfully doped dimensionally stable S-SEBS membranes (Stenina et al., 2020). Sulfonated SEBS (S-SEBS), as with many sulfonated block copolymers, is a great candidate for producing desirable surface morphology. Due to flexible side chains and self-assembling

capabilities, it exhibits excellent microphase separation between the hydrophobic backbone and hydrophilic functional groups (H. S. Park & Hong, 2021). The Park & Hong study previously referenced found that partially sulfonated SEBS had well-ordered and connected ionic channels for proton transport (H. S. Park & Hong, 2021). Overall, SEBS can be blended with other polymers to improve their membrane characteristics (Müller et al., 2012).

A current discussion on advanced materials for membrane separation applications should include the emerging link with additive manufacturing. Additive manufacturing or 3D printing has garnered interest in water desalination technologies due to the flexible and efficient use of design and materials (Qian et al., 2022). As of now, 3D printing has mostly had commercial success in manufacturing spacers to improve flux and resistance to fouling/scaling (Khalil et al., 2021; Tijing et al., 2020). Aside from manufacturing spacers, there have been some successful applications of additive manufacturing in water technology. For example, Park et al. recently published their method for synthesizing thin film composite (TFC) polyamide (PA) membranes using a standard inkjet printer (M. J. Park et al., 2022). However, direct membrane fabrication using additive manufacturing is borderline nonexistent. Some companies such as NanoSun and Nanotech have had commercial success by directly 3D printing membranes with an electrospinning technique, which has been applied in water treatment plants (Soo, Ali, & Shon, 2021). However, electrospinning lacks the resolution to control the membrane's morphology beyond some regulation over the film thickness (Soo et al., 2021). This lack of sufficient resolution is one of the significant challenges facing direct membrane manufacturing with any traditional 3D printing method. Directly printed membranes will remain unachievable until additive manufacturing equipment can produce pore sizes on the order of microns. This research applied additive manufacturing within a framework for creating interpenetrating polymer networks (IPNs).

IPNs are blends of partially interlaced polymers that have been proposed for applications in ion exchange, pervaporation, and molecular transport, among others (Karak, 2012; Ma et al., 2020; Zhao et al., 2019). As opposed to homogeneous materials, blends are useful for creating highly stable phases without the need for chemical crosslinking thanks to the ability to combine and manipulate the desirable properties of the multiple polymer materials. In this methodology, Fused Deposition Modeling was used to produce polymer films that were subsequently grafted with monomers and sulfonated using traditional fabrication methods.

Chapter 3: Experimental Methodology

The objective was to sulfonate extrusions of blended Styrene-Ethylene-Butylene-Styrene (SEBS) and Acrylonitrile Butadiene Styrene (ABS). An attempt to directly sulfonate the samples was made, but the pristine blends did not withstand the aggressive nature of the sulfonation reaction. Thus, a step for grafting the extrusions with crosslinked polystyrene was incorporated. Figure 3.1 shows the resulting two-step methodology.

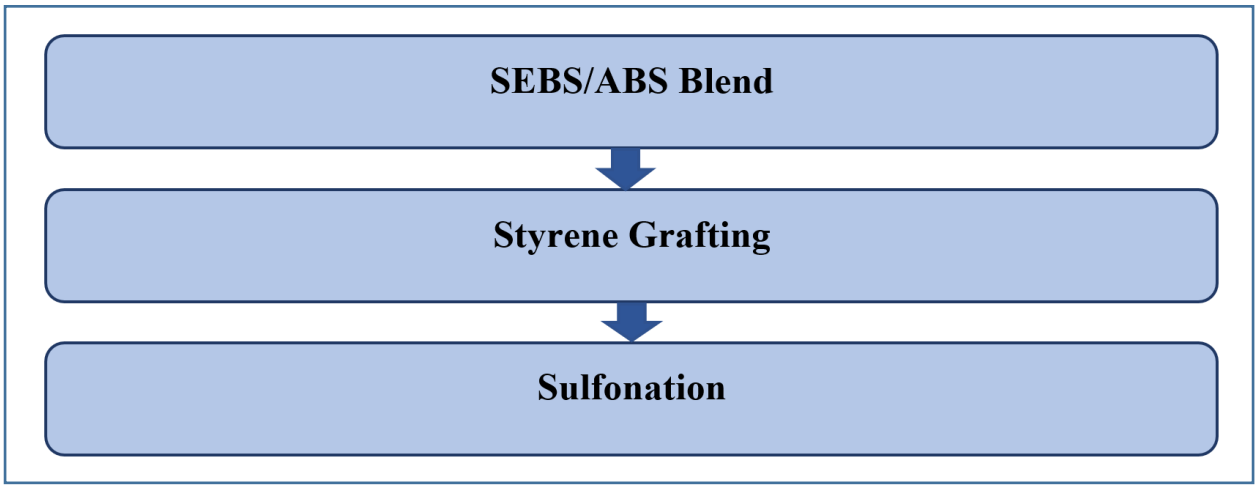

Figure 3.1 *Simplified methodology*

To graft the polystyrene, the polymer blends were immersed in a 90:10 mixture of styrene (STY) and divinylbenzene (DVB) and polymerized in-situ with heat treatment. Subsequently, the styrene-grafted samples were sulfonated with a 10:90 mixture of chlorosulfonic acid (CSA) and swelling solvent. Within the resulting two-step method, the grafting reaction was improved by adding various concentrations of benzoyl peroxide (BPO) to function as a polymerization initiator and crosslinking agent (Salazar Cruz, Rivera-Armenta, Esquivel De La Garza, Morales-Cepeda, & Ramos-Galvan, 2018). Additionally, the sulfonation reaction was improved by repeating the method with three different sulfonation solvents: dichloroethane (DCE), dichloromethane (DCM), and chloroform (CHL).

3.1 MATERIALS

Powdered 37.0% (w/w) Styrene SEBS A1536 HU, was purchased from Kraton (Houston, TX, USA). ABS CYCOLAC resin MG94 was purchased by Sabic (Pittsfield, MA). These polymers were blended with a 50:50 by-weight ratio and extruded with a Model ZK 25 T, Dr. Collin GmbH, Ebersberg, Germany twin screw extruder/compounder. The blend was developed by Torrado et al. as an FFF-compatible material. The monofilament was made with a diameter of 2.85 mm to be compatible with most desktop- and industrial-grade material extrusion 3D printers. The filament was extruded with a Lulzbot Mini FFF machine (Aleph Objects Inc., Loveland, CO, USA) with a nozzle tip size of 0.6 mm.

For the grafting of monomers, 99% extra pure styrene, MW=104, 15 was purchased from Acros Organics; technical grade 80% divinylbenzene was purchased from Aldrich Chemistry; benzoyl peroxide, 98% wetted with ca. 25% H2O was purchased from Frontier Scientific. The WVR Oven F Air 2.3 C.F. by Thermo Electron LED GmbH Robert- Bosch-Strasse 1, Langenselbold, Germany, was used to heat the samples.

For sulfonation, chlorosulfonic acid from Aldrich Chemistry was purchased. The solvents used were purchased as follows: Chloroform high purity solvent (without Ethanol) from Baxter Burdick and Jackson; 1,2-Dichloroethane (Ethylene Dichloride) reagent from Spectrum Chemical MFG Corp, ASCS; and Dichloromethane from BHDX. Sodium Bicarbonate in white crystalline powder form was purchased from Fisher Science for acid quenching, and the films were rinsed post-sulfonation with Methanol high-purity solvent from Burdick & Jackson. Figure 3.2 shows a schematic representation of the compounds used for styrene grafting and sulfonation.

Other chemicals purchased include crystalline Sodium Chloride and Sodium Hydroxide pellets from Fisher Science, Acetone from BDH, Hydrochloric Acid from SP Mallinckrodt, and

Phenolphthalein (1% in 95% Ethanol) indicator. All chemical reagents were used as purchased and were not further filtered.

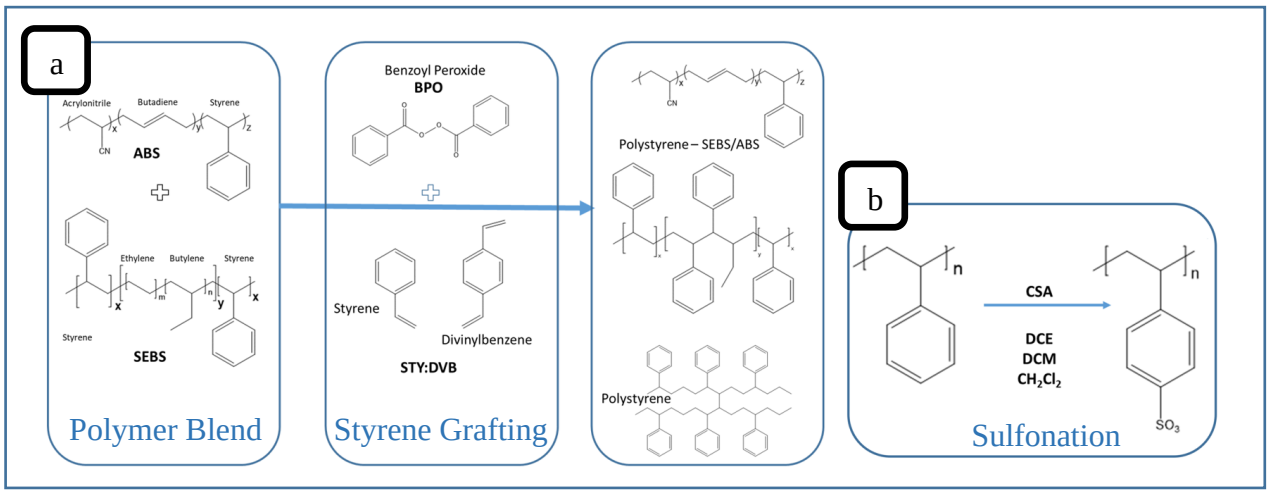

Figure 3.2 *Schematic representation of the grafting (a) and sulfonation (b) reactions*

3.2 3D PRINTING OF MEMBRANE SUPPORT

SEBS copolymer was blended with ABS thermoplastic to improve its form and rigidity. The blend was extruded with a Dr. Collin GmbH twin screw extruder into a monofilament with a diameter of 2.85 mm. The extruder was kept at 160° at T zone 1 and 165° at T Zones 2 through 5. The main screw operated at 70 RPM, the feed screw operated at 6% of the main screw, and the polymer mixture was fed at a pressure of 45 bar. The monofilament was printed using the material extrusion (ME) or fused deposition modeling (FDM) method on an FDM LulzbotTaz desktop 3D printer with a 0.6 mm nozzle. The shape and dimensions of the membrane were established in modeling software, and the printing parameters were set as follows: height of each layer of 0.2 mm with a 100% infill; feed rate of 40 mm/s; travel feed rate of 55 mm/s; print temperature of 230°C; and filament diameter of 1.9 mm. The methodology for extruding these SEBS:ABS blends was patented at the University of Texas at El Paso and the blends have been characterized in

previous publications (Rocha et al., 2014; Schnittker, Paso, & Gilberto Siqueiros, 2016; Torrado et al., 2015; Torrado Perez, Roberson, & Wicker, 2014; Patent No. US 10,954,369 B2, 2021).

3.3 MEMBRANE PREPARATION

The 3D printed films were first grafted with 10% crosslinked polystyrene using the in-situ copolymerization method to form a close connection between the support material and new aromatic rings (S. Jiang & Ladewig, 2017). The films were introduced to a homogeneous mixture of styrene and divinylbenzene monomers with benzoyl peroxide by immersing them in the solution for five to ten minutes until the films began to warp. Then the solution was removed, and the monomers soaked into the membrane support were polymerized for 8 h at 80°C. After the reaction, the membranes were delaminated with DI water, thoroughly rinsed, and dried for 12 hours.

Next, the styrene-grafted membranes were sulfonated with chlorosulfonic acid. The membranes were immersed in a 10:90 CSA/halogenated solvent solution for 5 minutes to obtain peak sulfonation and limit chain degradation. Subsequently, they were quenched with methanol, neutralized with a sodium bicarbonate solution, rinsed, and dried for 12 hours. Figure 3.3 shows the iterations of grafting and sulfonation solvents that were prepared.

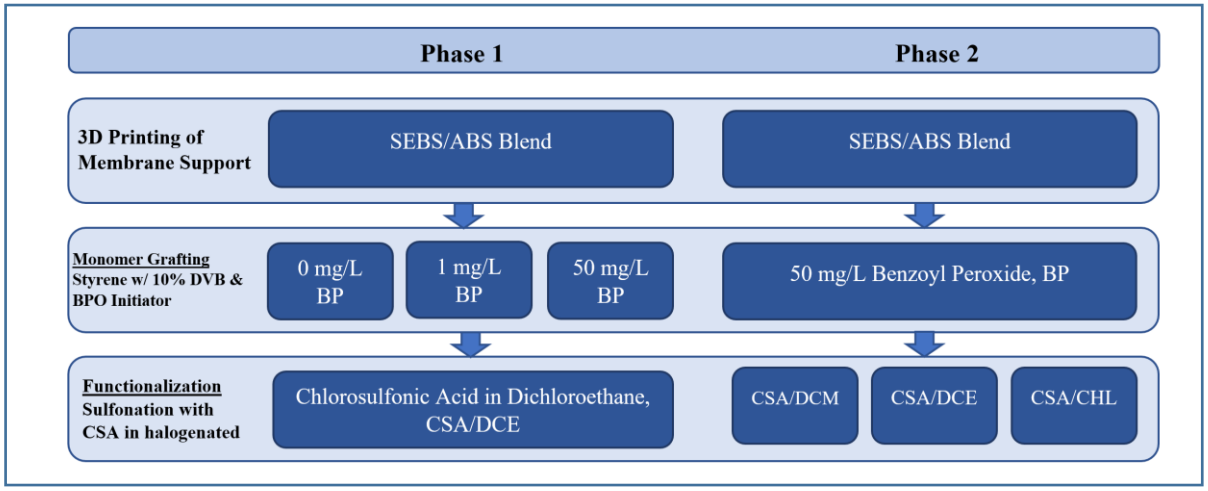

Figure 3.3 *Methodology*

3.4 CHARACTERIZATION METHODS

3.4.1 Ion Exchange Capacity (IEC) & Energy Dispersive X-ray Spectroscopy (EDX)

The ion exchange capacity (IEC) represents the exchange sites integrated into the final functionalized matrix. The titration method for approximating total IEC was adopted. After sulfonating the SEBS/ABS films, they were dried and weighed. Then they were conditioned in excess of 1M HCl solution for 24 hours and rinsed with DI water to remove the acid from the surface. Next, they were equilibrated in a 2M NaCl solution for 24 hours to allow the functionalized films to exchange their mobile hydrogen ions for the higher affinity sodium ions. When converting the films from the H^+ to the Na^+ form, H^+ ions were released into the solution; the released H^+ ions were measured via titration to represent the amount of active functional groups. That solution was titrated with 0.01M NaOH and phenolphthalein as an indicator. The IEC in meq/g was calculated with Equation 1, where C_{NaOH} is the concentration of the NaOH titrant solution, V_{NaOH} is the volume of titrant used, and W_{dry} is the dry weight of the membrane in the H^+ form:

[Equation 1] $$\text{IEC}\left(\frac{\text{meq}}{\text{g}}\right) = \frac{C_{NaOH} \times V_{NaOH}}{W_{dry}}$$

The data obtained from the ion exchange capacity titration was complimented with the elemental compositions acquired from EDS.

3.4.2 Fourier Transform Infrared (FTIR)

Fourier transform infrared (FTIR) analysis was conducted using a Nicolete™ iS™ 5 FTIR equipped with an iD7 attenuated total reflectance (ATR) Diamond (Thermo Fisher Scientific, Waltham, MS, USA). In FTIR, infrared radiation beams pass through a sample and produce vibrations as they interact with the molecular bonds of the sample to stretch, compress, or bend

them. The instrument measures the difference in optical pathways as they interact constructively or de-constructively with each other and converts those measurements from the time domain to the frequency domain using Fourier transforms. The locations and shapes of peaks in the resulting wave (cm^{-1}) vs. intensity plot are used to identify the presence of particular chemicals and functional groups in the sample. FTIR analysis was used to confirm the successful incorporation of styrene and sulfone groups. All FTIR data were normalized by dividing the signal output by the intensity of the highest peak in the series.

3.4.3 Scanning Electron Microscopy (SEM)

SEM imaging revealed the surface morphology of the ion exchange films. The SEM images were taken with a Hitachi SU 3500 SEM (Hitachi High Technologies America, Dallas, TX, USA) equipped with a backscatter electron detector (BSE) in variable pressure mode and an accelerating potential of 10 kV. The images taken after styrene grafting and after sulfonation were examined to compare the microphase separation of the polymer blend.

3.4.4 Small-angle X-ray Scattering (SAXS) & Wide-Angle X-ray Scattering (WAXS)

X-ray scattering was used to examine the crystallinity and phase expansions of the samples. SAXS and WAXS measurements of the dry films were carried out with a Xenocs Xeuss 2.0 HR SAXS/WAXS system (Sassenage, France) with a Cu source of λ=0.1542 nm, sample detector distance of 1202.2 mm, and collection time of 2 x 1800s per sample. The x-rays were scattered and collected on the detector as a function of the scattering angle (2θ) with respect to the transmitted direct beam. The 2D scattering patterns were azimuthally averaged to obtain the intensity, I(q), as a function of the wave vector, $q=4\pi\lambda^{-1}\sin\theta$.

Chapter 4: Results and Discussion

In this research, the electrochemical properties and morphology of styrene-grafted sulfonated SEBS (S-SEBS-g-styrene) were explored with respect to two variables: the concentration of benzoyl peroxide as the initiator during the in-situ graft copolymerization reaction, and the sulfonating agent/solvent combination used in the sulfonation reaction. These variables were independently tested in experiments 1 and 2 on the 3D-printed SEBS/ABS blends. The films were grafted with a 90% styrene and 10% divinylbenzene monomer solution, and polymerization within the SEBS/ABS substrate was triggered by heat treatment. The grafted material was then sulfonated with chlorosulfonic acid in a halogenated solvent. Once these films were functionalized for ion exchange, they were characterized with two goals: to analyze (and maximize) the effects of the variable chemistries on the incorporation of functional sulfone groups and to observe favorable macro and micro morphology of the post-sulfonated material.

Experiment 1 aimed to achieve more successful polystyrene grafting to increase the incorporation of sulfonation-eligible styrene rings in the ethylene-butylene portion of the polymeric matrix. Although the ethylene-butylene mid-blocks in SEBS contribute to its excellent thermal stability and chemical performance, only the styrene repeat units provide attachment locations for the sulfone groups that functionalize the inert material for ion exchange. In this study, an attempt to control the degree of grafting was made by adding different concentrations of benzoyl peroxide (BPO) initiator to the solution of monomers. In the polymer matrix, these ion exchange films were characterized in their pre- and post-sulfonation states to quantify the degree of styrene and sulfone group incorporation. Ion exchange capacity measurements and FTIR spectroscopy confirmed the incorporation of styrene and sulfone groups.

In experiment 2, the aim was to achieve more effective sulfonation by modifying the chemical reagents of the sulfonation reaction. In this reaction, the chemical reagents are usually the sulfonating agent and the swelling solvent. While sulfuric acid can play the role of both, other sulfonated reagents, such as chlorosulfonic acid (CSA), need to be paired with a separate swelling agent. The purpose of the solvent is to simultaneously dissolve a degree of the electrophile (i.e., the sulfone groups provided by the sulfonating agent) and the polymer matrix to enable a reaction between the two. Dichloroethane (DCE), dichloromethane (DCM), and chloroform (CHL) are three commonly used solvents, though the effects of using one solvent over another have not been widely studied. In this study, the effect of the sulfonation solvent was analyzed for the degree of sulfone group incorporation in the polymer matrix. Ion exchange capacity measurements and FTIR spectroscopy confirmed the incorporation of sulfone.

The second goal of the investigation was to observe the surface morphology of all the ion exchange films produced during experiments 1 and 2. One of the biggest challenges of sulfonating materials is that the swelling necessary for the functionalization reaction can aggressively destroy the base polymer's morphology. This investigation observed similar damage to the polymer's integrity after grafting with polystyrene. Our sulfonated SEBS/ABS films were visualized at the macro and micro scale to determine the chemical conditions that best preserved the morphologic integrity. On the macro-scale, samples were evaluated for the preservation of the homogeneity and orientation of the original 3D printed material. On the micro-scale, samples were evaluated for achieving highly separated phase morphology (distinct hydrophilic and hydrophobic domains), well-distributed sulfone clusters, and interconnected, structurally ordered, and globular channels. SEM Imaging and Small Angle X-Ray confirmed these macro and micro properties.

4.1 Ion Exchange Capacity (IEC) & Energy Dispersive X-ray Spectroscopy (EDX)

Analysis of the extent of the graft polymerization and sulfonation reactions began with estimations of the elemental composition via EDX and ion exchange capacity via titration. The presence of sulfur in the post-sulfonated specimens was confirmed by elemental composition analysis with EDX.

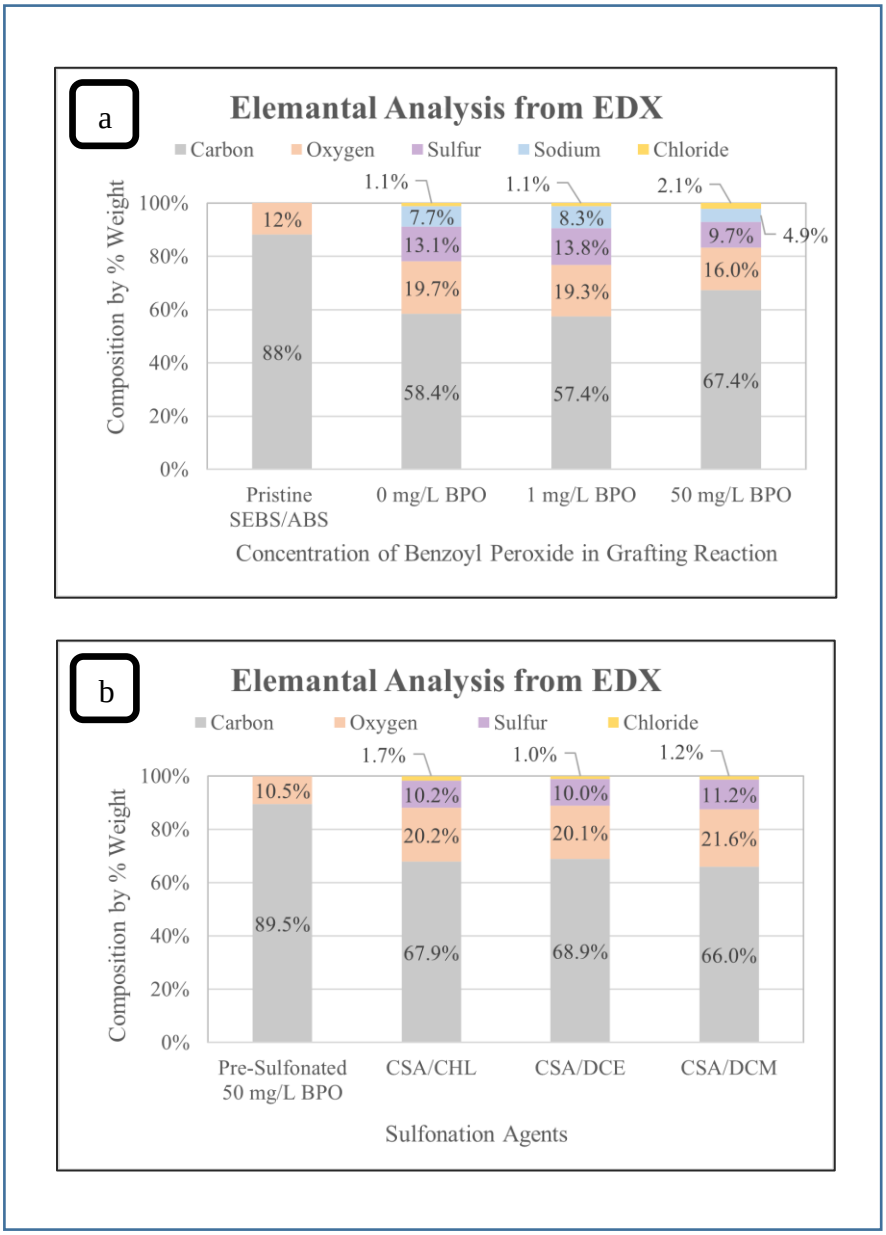

Figure 4.1 *Elemental composition of sulfonated SEBS:ABS samples for different chemistries of grafting with benzoyl peroxide (a) and sulfonation with CSA in halogenated solvents (b)*

Elemental contents were estimated via EDX by the ion exchange films' percent weight of C, O, S, and Cl. Specimens from experimental group 1 (benzoyl peroxide variations) were analyzed in the Na+ form (containing Na+ counterions), so EDX also produced weight percentages for elemental Na. Figure 4.1 shows the results from EDX for the post- sulfonated samples of both experimental groups.

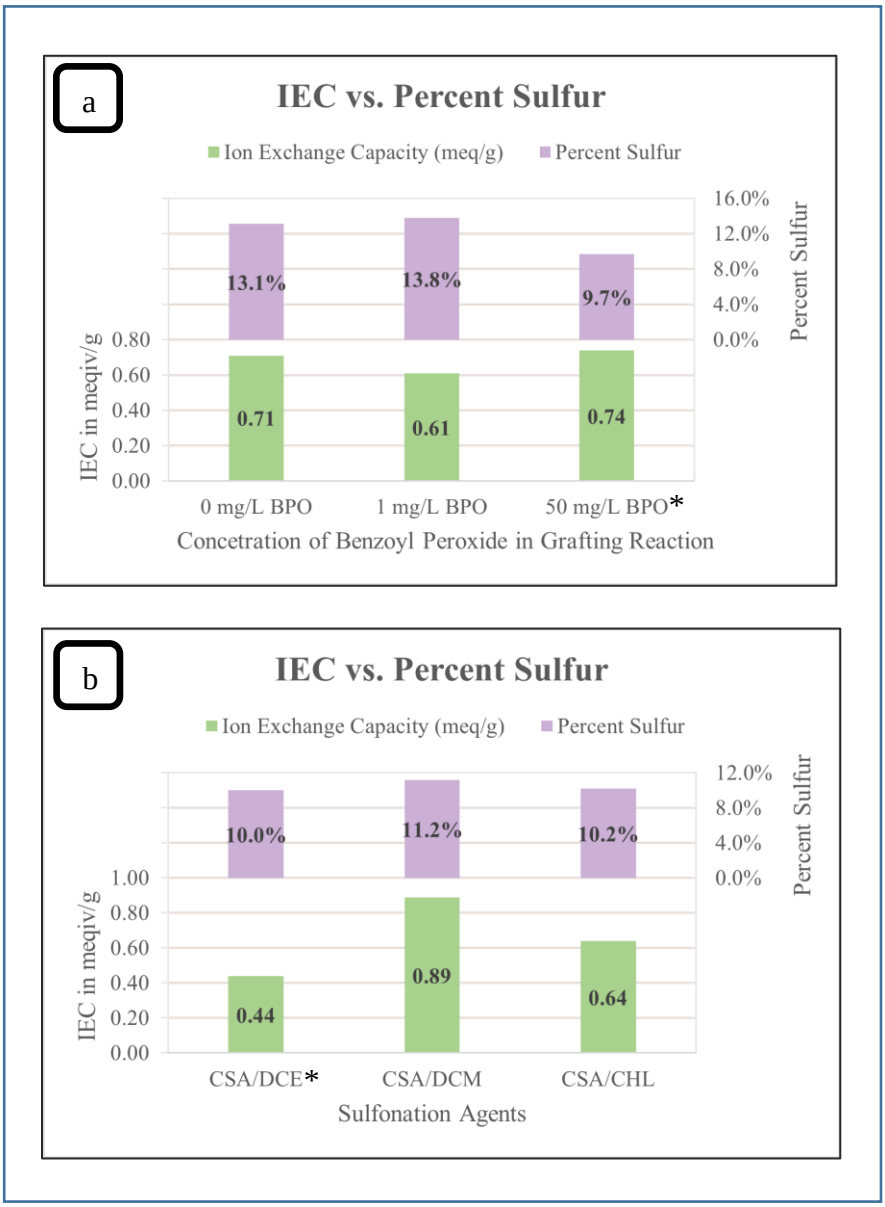

Figure 4.2 *Sulfur content (EDX) and ion exchange capacity (titration) of sulfonated SEBS:ABS samples for different chemistries of grafting with benzoyl peroxide (a) and sulfonation with CSA in halogenated swelling solvents (b)*

Figure 4.2 compares the sulfur percentage values (%S) from EDX alongside the ion exchange capacity (IEC) values obtained by the titration method. In the first experimental phase, the sample with the highest quantity of benzoyl peroxide (BPO) had the highest IEC.

The higher IEC was attributed to more active functional groups in the ion exchange material and more aromatic styrene rings in the polymer chain as a precursor. Thus, it was concluded that the higher quantity of initiating compound in the grafting copolymerization reaction was responsible for a certain degree of successful grafting. Interestingly, the IEC of the 1 mg/L BPO sample was lower than the sample with no added BPO. This anomaly was attributed to a chemical inhibitor in the benzoyl peroxide. The low concentration of BPO was likely too weak to encourage a strong polymerization reaction to overcome the inhibitor's effects. Therefore, relative to the simple styrene/divinylbenzene solution, adding 1 mg/L of BPO had a negative effect on the success of grafting.

In the second experimental phase, the sample sulfonated with CSA in DCE had the lowest ion exchange capacity, and the sample sulfonated with CSA in DCM had the highest ion exchange capacity. The lower ion exchange capacity produced by DCE indicates that, in terms of desirable conductive properties, it was a less effective sulfonating solvent than its DCM and CHL counterparts. However, this may also be interpreted as an indication of a less aggressive and destructive sulfonation reaction. This conclusion was further corroborated when the morphology of the membranes was evaluated with SEM imaging.

The ion exchange capacity obtained experimentally by titration is a proxy measurement of the sulfone groups incorporated into the polymer matrix. Theoretically, the amount of elemental sulfur detected by EDX should be positively correlated with the IEC value. However, a direct comparison should be approached with caution. For example, a study published by Nagarale et

al., which explored the effects of sulfonation solvents on simple polysulfone material, calculated the extent of sulfonation by H-NMR spectroscopy, CHN elemental analysis, and titration (IEC). In their data, the ion exchange capacity was loosely correlated to the incorporation of functional groups found via spectroscopy but inversely correlated with the extent of sulfonation in the matrix estimated from elemental analysis. In that particular case, the inverse relationship between percent sulfur and IEC was attributed to the cleaving of the polymer chain caused by some of the solvents studied (Nagarale et al., 2005). Similar nuances in the data presented are discussed in the following paragraphs:

First, the samples marked by an asterisk in Figure 4.2 were made with the same grafting and sulfonation chemistry– SEBS:ABS polymer grafted with a 90% styrene-10% divinylbenzene-50 mg/L benzoyl peroxide mixture and sulfonated with 10% chlorosulfonic acid in dichloroethane. The IEC of these samples was 0.74 meq/g in the first experimental phase and 0.44 meq/g in the second experimental phase. This disparity could be attributed to a longer sulfonation time in the first experiment (approaching 10 minutes versus the 5 minutes applied the second time). Thus, it was determined that the quantitative analysis of these two data sets should be performed independently.

Second, the IEC and percent sulfur are negatively correlated in the first and positively correlated in the second data set. It is possible to attribute this to the same factor previously mentioned– the difference in sulfonation times between the first and second sample sets. While longer sulfonation times cause higher sulfonation, this does not necessarily correlate to more active exchange sites. The longer sulfonation time may have begun to destroy some of the styrene locations in the polymer chain available for sulfonation, thus reducing the ion exchange capacity. Alternatively, higher incorporation of sulfone groups, which leads to closer proximity between

them, may have sterically hindered the functionality of the exchange sites. However, because the elemental compositions are percentages by weight and not absolute values, and because the samples were in different counterion forms when EDX was applied, conclusions about the sulfonation-IEC relationship in these samples were not definitive.

4.2 FTIR-ATR

The first important peaks in the pristine SEBS:ABS sample occur in the 2800-3200 cm^{-1} range. These characteristic SEBS and ABS peaks correspond to aromatic (3000-3200 cm^{-1}) and aliphatic (2800-3000 cm^{-1}) C-H stretching (Müller et al., 2012).

Multiple low-intensity bands characteristic of C-H aromatic stretching (3000-3200 cm^{-1}) are present with approximately equal intensities in the pristine and styrene-grafted samples (Figure 4.3a). The disappearance of the peaks in the sulfonated samples (Figures 4.3b and 4.4) was attributed to the successful attachment of sulfone groups to the aromatic locations.

For the C-H aliphatic stretching (2800-3000 cm^{-1}), two peaks corresponding to asymmetrical and symmetrical CH_2 stretching are present in the pristine, styrene-grafted, and sulfonated samples (S. Jiang & Ladewig, 2017; Yan et al., 2021). In the first experimental phase, when compared to pristine SEBS:ABS, the intensities of the two peaks were drastically weakened in the sample grafted with 0 mg/L BPO. This peak reduction might indicate that the monomer grafting reaction without a chemical initiator partially destroyed the ethylene-butylene portion of SEBS and the butadiene portion of ABS. The higher peaks in the 1 mg/L and 50 mg/L samples show that aliphatic C-H from pristine SEBS and ABS was preserved more with increasing amounts of benzoyl peroxide. In fact, the sample grafted with 50 mg/L produced a signal slightly more enhanced from the pristine polymer blend. This enhanced signal revealed that the higher levels of

grafting achieved with benzoyl peroxide protected the butadiene (from ABS) and ethylene-butylene (from SEBS) polymer domains from the harsh effects of chemical solvents. This polymer preservation granted by benzoyl peroxide was further observed when the samples were sulfonated (Figure 4.3b). After being sulfonated with CSA in DCE, the aliphatic C-H peaks for the 0 mg/L BPO and 1 mg/L BPO samples were largely destroyed, indicating very little -EB- of ABS phases remaining in the material. The 50 mg/L BPO sample was the only chemistry that preserved the CH_2 groups in the original SEBS and ABS polymers. In the second experimental phase, the samples were all grafted using the 50 mg/L benzoyl peroxide concentration and then sulfonated with chlorosulfonic acid in dichloroethane, dichloromethane, and chloroform, respectively. After sulfonation, the C-H aliphatic peaks were best preserved in the following order: CHL<DCM<DCE. Dichloroethane and dichloromethane were less destructive of the ABS phase than chloroform, the latter which almost annihilated the C-H aliphatic peaks.

The weak 2238cm^{-1} peak characteristic of CN acrylonitrile is present in the pristine, styrene-grafted, and sulfonated samples (Desrousseaux et al., 2015). The peak was slightly reduced in the samples treated with 50 mg/L BPO.

Evidence of successfully grafted styrene was found by observing characteristic polystyrene peaks located in the 1300-1600 cm^{-1} region (C=C stretching) and 900-1050 cm^{-1} region (C-H in-plane bending) (Müller et al., 2012).

Multiple medium-intensity peaks, approximately centered at 1500 cm^{-1}, corresponding to aromatic C=C stretching occur in the pristine SEBS sample. Compared to the post-grafted (but pre-sulfonated) profiles from Figure 4.3a, the intensity of these peaks stays relatively constant across the samples. However, there is a notable increase in the number of peaks as a function of higher benzoyl peroxide concentration. The new peaks around 1300-1600 cm^{-1} that appear in the

50 mg/L BPO profile not only enhance the C=C aromatic stretching region but also enter the 1650-2000 cm^{-1} region of aromatic compound C-H bending that is characteristic of benzene rings (Smith, 2016). These new peaks observed in the 50 mg/L BPO sample were ascribed to incorporating additional styrene groups into new locations in the polymer chain. The new styrene locations were interpreted as evidence of successfully adding styrene groups to the ethylene-butylene portion of SEBS, where styrene locations did not exist prior to grafting.

In the pre-sulfonated samples, a small, unexpected peak appears at approximately 3300 cm^{-1} in the 1 mg/L sample and becomes more intense in the 50 mg/L samples. Because this small peak appears at almost double the wavenumber of the new peaks in the C-H aromatic bending region (1650 cm^{-1}), it may be an overtone band corresponding to those new polystyrene peaks (Smith, 2016).

The sulfonation reaction produces distinct characteristic peaks in two regions observed in Figures 4.3b and 4.4. The first corresponds to the intensified peaks at 900-1200 cm^{-1}. The peaks in this region can be attributed to the following vibrations in order of highest (~1200 cm^{-1}) to lowest (~900 cm^{-1}) wavenumber: the asymmetric and symmetric S=O stretching vibrations caused by the bonds of the newly incorporated sulfonic groups, C-S stretching, and the symmetric stretching of $–SO_3^-$ groups (Müller et al., 2012; Yan et al., 2021). Peaks for C-H out-of-plane bending in the lowest wavenumbers were also stretched due to the sulfonation reaction. The second characteristic peak of successful sulfonation is observed in the 3600-3300 cm^{-1} region (H. S. Park & Hong, 2021). The broad and weak absorption band observed in the sulfonated samples indicates the presence of hydroxy (–OH) species from the SO_3H groups. In the samples from peaks in both regions related to sulfonation.

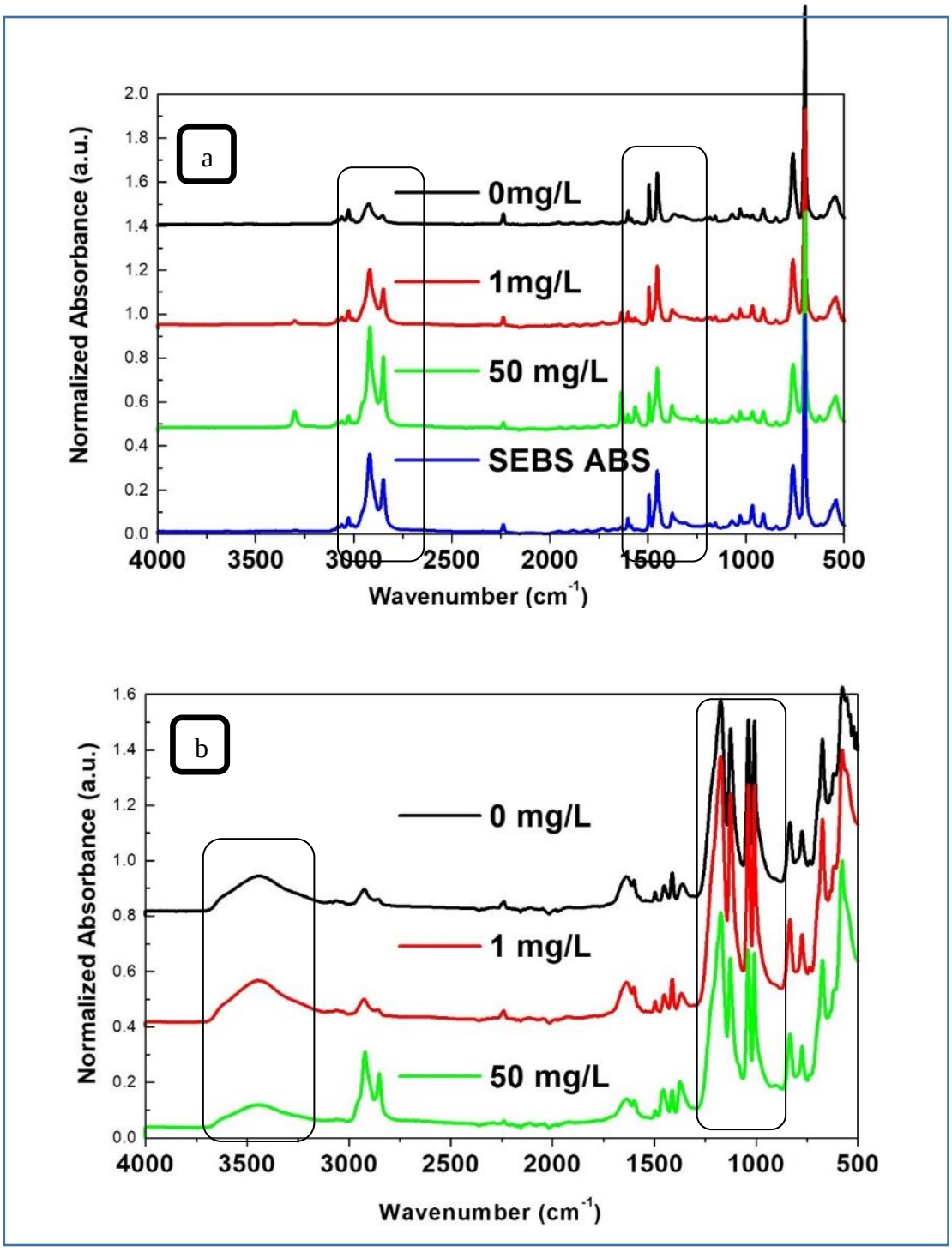

Figure 4.3 *FTIR-ATR Spectra for samples grafted with various BPO quantities in their post-grafted (a) and post-sulfonated (b) states*

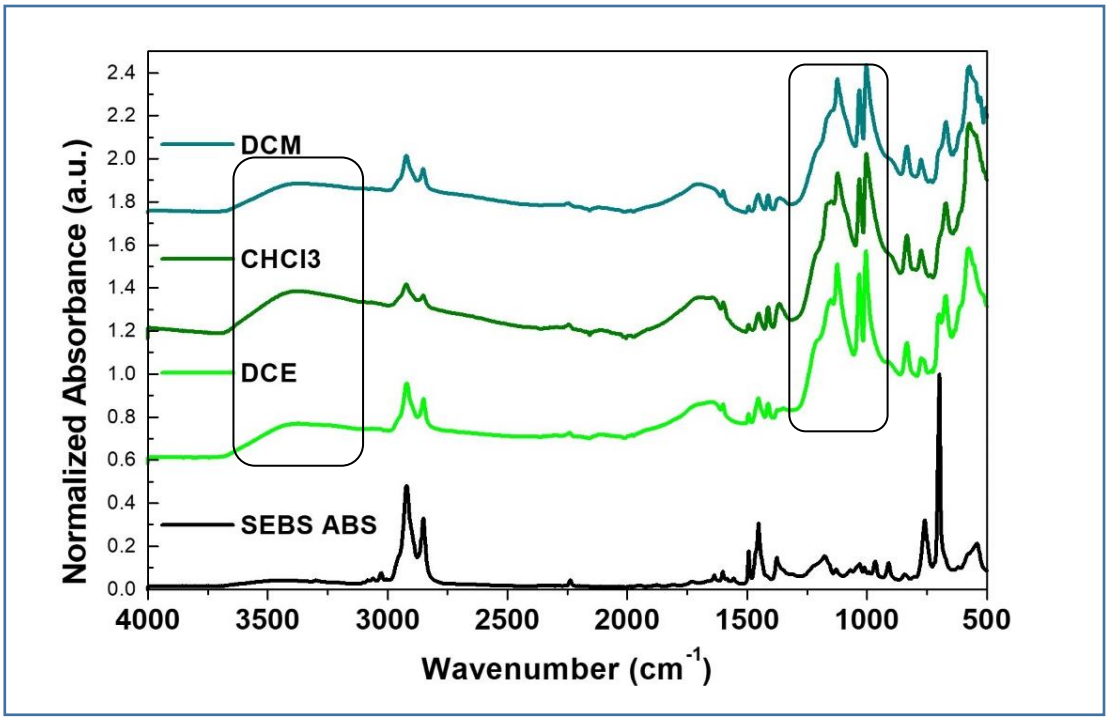

Figure 4.4 *FTIR-ATR Spectra for samples sulfonated with various solvents*

4.3 SCANNING ELECTRON MICROSCOPY (SEM)

SEM analysis was used to visualize the different chemical compositions in the specimens by imaging the contrast generated by the energy feedback of differing polymer phases. The preceding study at the UTEP Department of Metallurgical and Materials Engineering department, which developed the methodology for 3D printing SEBS and ABS into an IPN, characterized the binary blend using a scanning electron microscope. Through SEM analysis, they confirmed a degree of miscibility of ABS in SEBS and noted the comparatively smoother cross-sectional planes in the deposition morphology, as opposed to a pure ABS specimen. In the current investigation, SEM imaging was used to visualize the changing top surface morphologies of these SEBS:ABS films during the polystyrene grafting and sulfonation reactions.

The phases of different polymers species are distinguished in these micrographs by the changes in image color. Figure 4.5 shows the micrograph of the pristine SEBS:ABS material, as

evidenced by the unaltered deposition lines from printing. Although the microstructure of the pristine SEBS:ABS film confirmed adequate miscibility of the copolymers, small (~50 µm) but distinguishable domains were observed. The pore-like microdomains and randomly distributed white zones were attributed to phase separation between ABS and SEBS (Müller et al., 2012).

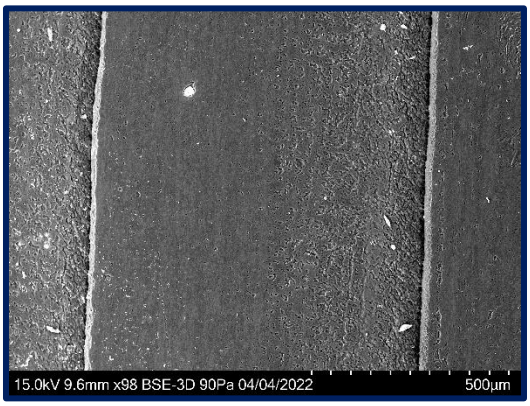

Figure 4.5 *SEM micrograph for pristine SEBS:ABS extrusion*

Figure 4.5 displays the micrographs for the films after styrene grafting with 0 mg/L, 1 mg/L, and 50 mg/L concentrations of benzoyl peroxide in their pre-sulfonated (a, b, and c, respectively) and post-sulfonated (a', b', and c', respectively) state. In all three samples, styrene grafting caused significant changes in the phase separation and homogeneity of the polymer blend. However, in the samples grafted with a monomer blend containing 0 mg/L and 1 mg/L of benzoyl peroxide, severe separation and deconstruction of the polymer phases were observed even before sulfonation. After sulfonation, the loss of polymer domains was intensified. The reduction in different polymer phases corroborates the FTIR findings that showed that the compounds of the grafting and sulfonation reactions aggressively dissolved the polymer matrix, almost completely evaporating the ABS out of the blend. Furthermore, the aggressive sulfonation caused external surface cracks similar to those observed in micrographs of commercial styrene-divinylbenzene copolymer resins (De Oliveira et al., 2005).

On the other hand, the micrographs for the sample grafted with a monomer blend containing 50 mg/L of benzoyl peroxide show a drastic change in the separation patterns. In the post-grafted state, the polymer domains are larger than in the original pristine extrusions because the polystyrene is partially miscible in the SEBS domains, increasing the latter in size (Banerjee, Ray, & Ghosh, 2018). However, unlike the previous two samples, the domains are separated and distinguishable. In the post-sulfonated state, the increase in the intensity of the dark phase suggests that these areas were sulfonated (heavier molar mass of sulfur and oxygen atoms). Preservation of the multiple polymer species is evident by the separated phases. This preservation of ABS because of increased graft polymerization initiator was particularly remarkable due to ABS's poor swelling resistance to aromatic hydrocarbons, sulfuric acids, and chlorinated solvents (Edwards, 2007).

Figures 4.7b, 4.7c, and 4.7d show the samples sulfonated with chlorosulfonic acid in dichloroethane, chloroform, and dichloromethane, respectively. The magnifications show that sulfonation with dichloroethane was advantageous over dichloromethane and chloroform in two ways: more clearly defined and uniformly dispersed polymer domains and an overall preservation of the linear appearance of the pristine and styrene-grafted material. In both the grafted and sulfonated phases, the CSA/DCE sample resulted in enlarged domains compared to the pristine material but smaller (~150 μm) and more linearly ordered domains than the CSA/DCM sample. Likewise, CSA/DCE appeared to best prevent the ABS from dissolving out of the blend, in contrast to the CSA/CHL sample, where the domains appeared to be slightly less defined. Moreover, the micrograph for the sulfonated sample with chloroform shows a major fracture at the bottom left corner. These results support that chloroform that the swelling action of chloroform was more aggressive on the morphology than the other solvents.

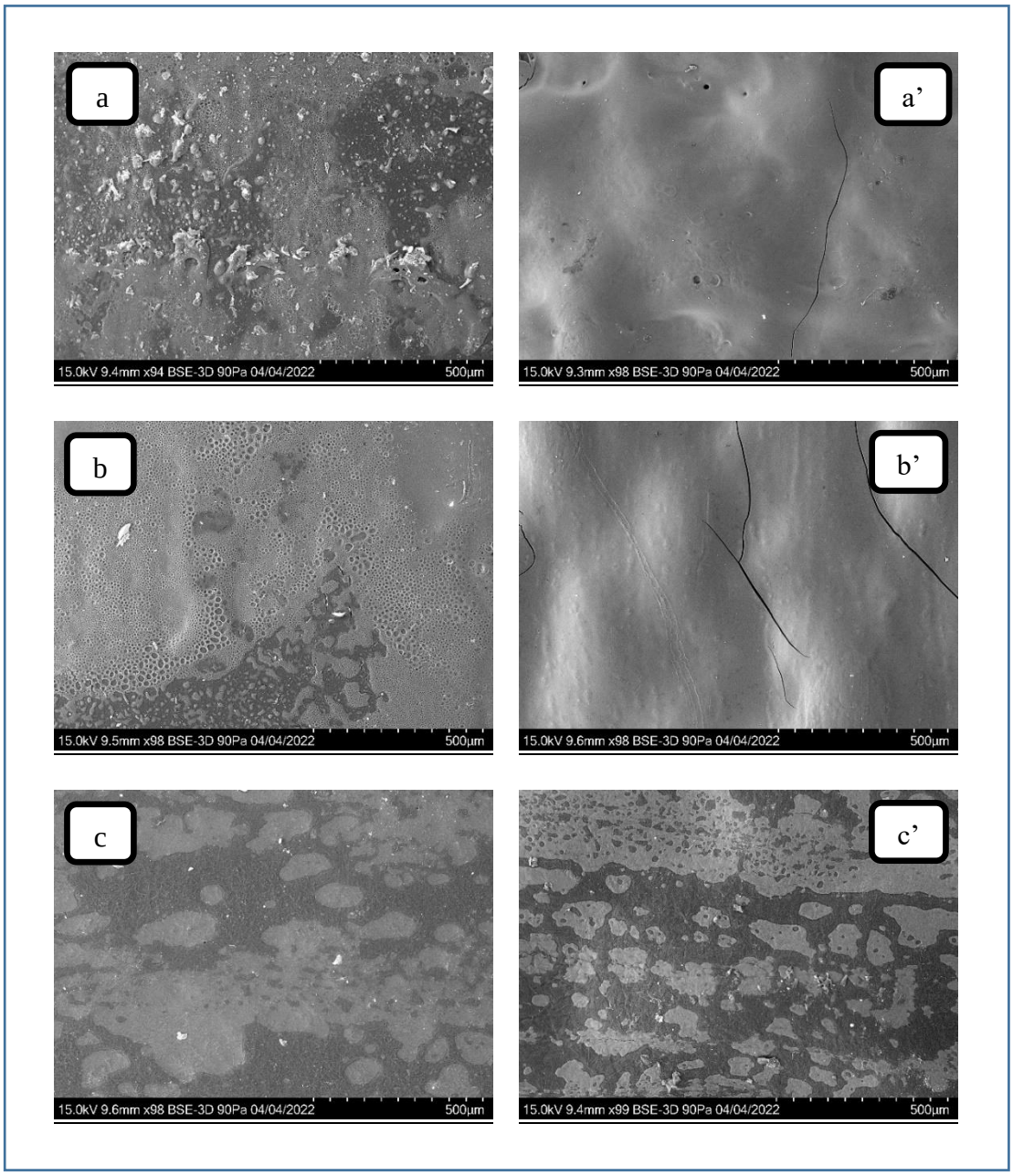

Figure 4.6 *SEM micrographs for samples grafted with 0 mg/L BPO post-grafted (a) and post-sulfonated (a'), 1 mg/L BPO post-grafted (b) and post-sulfonated (b'), and 50 mg/L BPO post-grafted (c) and post-sulfonated (c')*

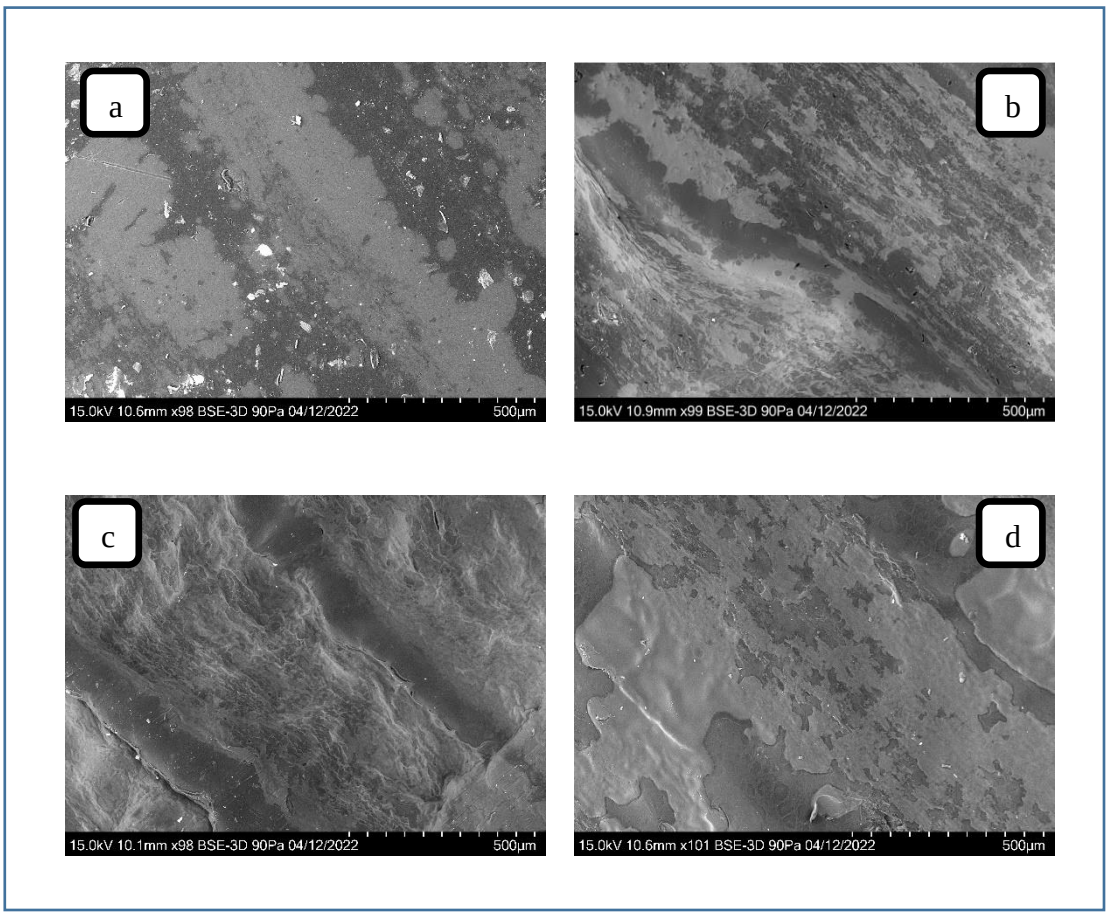

Figure 4.7 *SEM micrographs for samples grafted with 50 mg/L BPO (a) and sulfonated with dichloroethane (b), chloroform (c), and dichloromethane (d)*

These results suggested that dichloroethane was the best solvent for preserving the micromorphology of the 3D-printed polymer blend. However, the micrograph differences may have been marginal compared to the samples where the grafting reaction was varied. It should be noted that the solvent used in the sulfonation reaction had a less dramatic effect on the morphology imaging than the degree of styrene grafting. Designing for a higher degree of crosslinked styrene grafting proved to be the best option for preserving the polymer integrity and surface morphology in the SEBS:ABS extrusions.

4.4 SMALL-ANGLE X-RAY SCATTERING (SAXS) & WIDE-ANGLE X-RAY SCATTERING (WAXS)

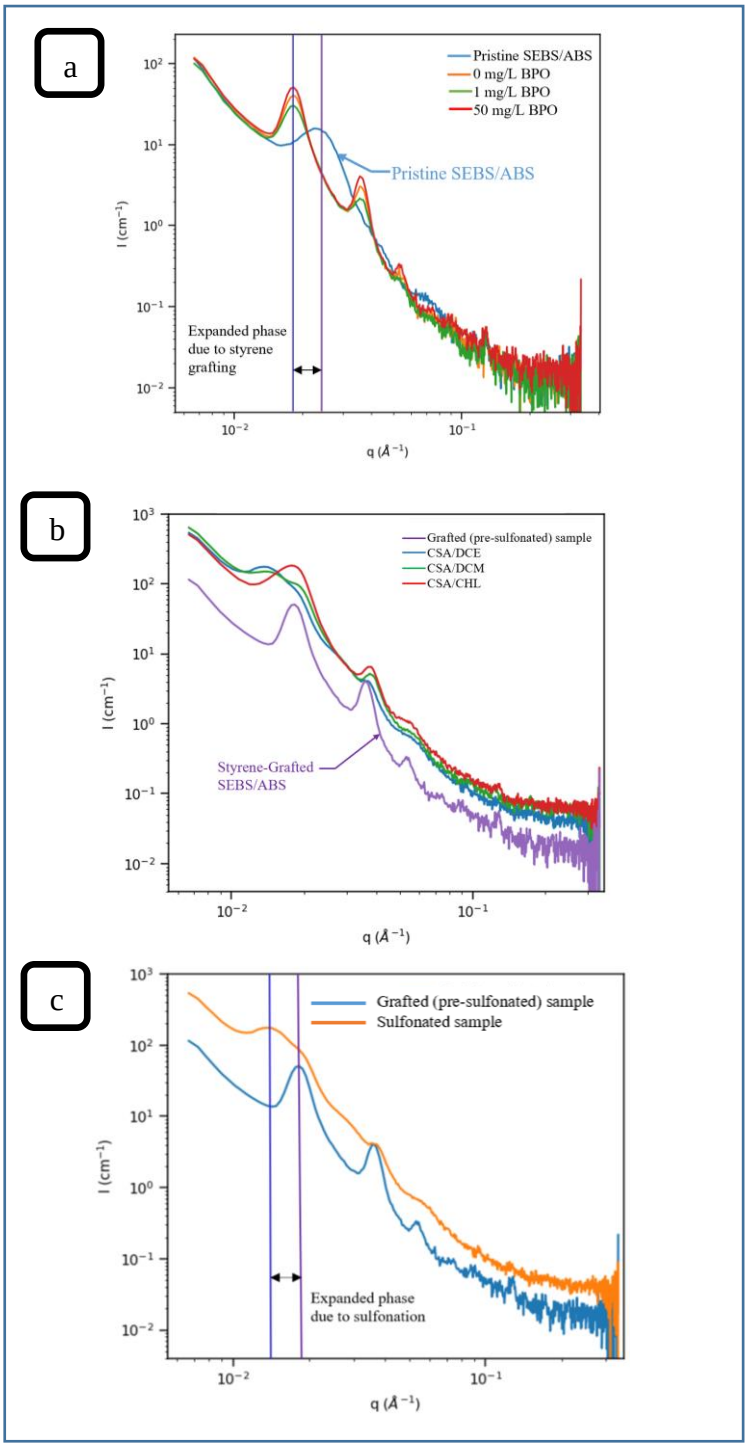

Figure 4.8 *SAXS intensity profiles for samples grafted with various BPO in their post-grafted (a) and post-sulfonated (b) states and for samples sulfonated with various solvents (c)*

SAXS and WAXS profiling was conducted to examine the structural domains of the styrene and sulfone groups. Figure 4.8 shows the SAXS profiles for the samples. While the peaks represented the presence of polystyrene domains, the distances between the peaks represent the center-to-center spacing between the domains. Expansions in the samples relative to the pristine material indicate the addition of new styrene or subsequent sulfone groups. The samples were qualitatively analyzed for changes in the position and relative sharpness of the nematic ordering peaks. A more narrowly dispersed or sharp peak indicated an increase in the crystallinity of the internal structure, while a broader peak suggested a less orderly internal structure.

Similarly, a rightward shift in the peaks was ascribed to smaller nematic packing, and a leftward shift was interpreted as larger interplanar distances between the domains. The WAXS profiles of the samples were relatively unchanging, as was the case in a previous investigation that also studied the properties of S-SEBS with x-ray scattering. The unchanging WAXS profiles indicated the aggregate styrene domains being stable under sulfonation and that the nano globular self-assembled aggregations could be defined from the SAXS intensity profiles (Orujalipoor et al., 2019).

Additionally, the assumption was made that the ABS in the samples did not contribute to the SAXS signals because of its amorphous and disorderly internal arrangement compared to SEBS. This rightful exclusion of ABS was confirmed by a baseline analysis of multiple purely cast SEBS samples and by the constant amount of SAXS peaks throughout the grafted samples, irrespective of whether the ABS phase had been preserved. Therefore, all the observations extracted from the intensity profiles were attributed to the SEBS polymer chain.

Figure 4.8a shows the SAXS intensity profiles for pristine SEBS and the samples grafted with different concentrations of benzoyl peroxide before sulfonation. The first and second nematic ordering peaks in the grafted samples show a distinct leftward shift after being grafted with polystyrene compared to the pristine sample. In other words, the interplanar distance between the styrene domains widened. FTIR analysis demonstrated that the grafting reaction added styrene domains to new locations on the ethylene-butylene portion of the SEBS chain. The leftward trend in the SAXS profiles for the same samples was interpreted as evidence of the newly grafted styrene domains tending to attach to the locations on the -EB- chain closest to the existing styrene groups. Among the different concentrations of benzoyl peroxide, the SAXS profiles clearly show that the 50 mg/L BPO sample produced the sharpest peak, while the 1 mg/L BPO sample produced the broadest peak. These sharper peaks supported the previous findings that the higher benzoyl peroxide concentration improved the material's morphology and that the lower concentration of benzoyl peroxide inhibited the polymerization reaction.

After sulfonation, the samples grafted with different degrees of benzoyl peroxide were also analyzed with SAXS. Figure 4.8b shows the 50 mg/L BPO after sulfonation with CSA/DCE. The expansion of the styrene peaks visually confirms that the sulfone groups were added to those styrene domains during the sulfonation reaction. However, modeling data demonstrated that the styrene domains in the sample were not all uniformly expanded. Some of the domains exhibited styrene expansion, while others did not. This uneven phase expansion confirmed the clustering phenomenon of the grafted styrene groups to the original styrene groups.

Figure 4.9 visually represents the detection of non-expanded and expanded phases. The non-expanded phase is similar to the state of the styrene domains before sulfonation. In the expanded phase, the radius of the group becomes measurably larger, indicating extra electron

density close to the styrene that is attributed to the attachment of the additional styrene. The expansion for this particular sample was calculated to be 41.7 Å, which may account for exactly two additional styrene groups, each of which has been estimated to be 20 Å in previous literature. Furthermore, the outer circle radius increase reflects an increase in the interplanar distance between the styrene groups. This phase expansion was interpreted as evidence of sulfonic group attachment to the styrene domains.

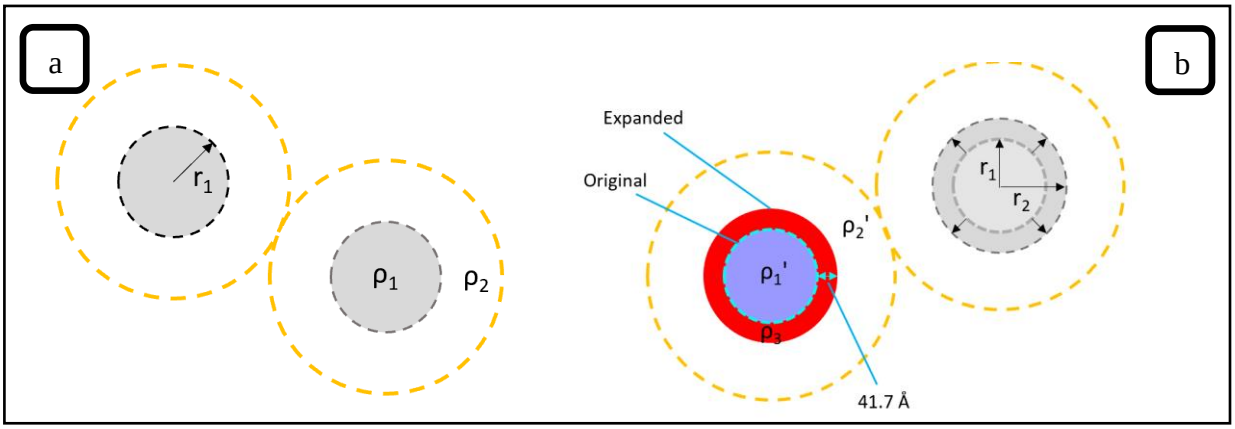

Figure 4.9 *Non-expanded (a) and expanded (b) phases of the styrene domains*

Lastly, the samples produced with different sulfonating chemistries were analyzed under SAXS. Figure 4.8c shows the profiles for these samples compared to the styrene-grafted sample before sulfonation. The profile for the sample sulfonated with CSA in chloroform had peak positions that were the most similar when compared to the unsulfonated sample. Referencing the larger sulfonation-related FTIR peaks in this sample, the sharper and more rightward SAXS peaks may corroborate that chloroform acted as the most potent sulfonating agent. These SAXS peaks may also support the smaller and less segregated domains observed in SEM analysis. Unfortunately, as was also shown in the SEM micrograph, the swelling action of chloroform was the most destructive to the integrity of the copolymer matrix.

Chapter 5: Conclusion

5.1 Conclusions of findings

In this work, we improved the morphology of SEBS functionalized for cation exchange applications. Working with an additive manufacturing technique, SEBS blended with ABS was grafted with crosslinked styrene to create an interpenetrating polymer network. The success of the grafting reaction was enhanced by adding different concentrations of benzoyl peroxide initiator. FTIR confirmed that a higher amount of benzoyl peroxide led to higher incorporation of styrene groups to new locations in the ethylene-butylene portion of the SEBS polymer chain. Because of the additional benzene aromatic rings, the sample was more extensively sulfonated. This greater extent of sulfonation was observed in the larger ion exchange capacity over the sample grafted with less benzoyl peroxide. More importantly, the increase in the degree of grafting caused by the higher benzoyl peroxide content significantly preserved the different polymer phases throughout the grafting and sulfonation reaction. The SEM micrographs showed how the ABS in the samples grafted without benzoyl peroxide underwent severe dissolution and evaporation during the styrene grafting reaction and, more drastically, during the sulfonation reaction. The significantly reduced FTIR peaks confirmed the destruction of ABS domains for C-H aliphatic of the pristine material after undergoing polystyrene grafting.

On the other hand, the ABS domains were exceptionally preserved when benzoyl peroxide was added to the grafting monomers. The SEBS and ABS domains were clearly present and distinctly separated in the SEM images for the samples in their post-grafted and post-sulfonated state. Significantly, this means the solvent resistance of ABS was greatly improved. Finally, SAXS profiles demonstrated that the higher degree of grafting increased the order and crystallinity of the hydrophilic/hydrophobic domains in the microstructure of the dry material.

The morphology of the sulfonated SEBS was further improved by changing the chemistry of the sulfonation reaction. Samples grafted with identical chemistries were sulfonated with chlorosulfonic acid in dichloroethane, dichloromethane, and chloroform. Chloroform was found to be the most intense swelling agent for sulfonation. This aggressive swelling action was confirmed by the more prominent characteristic sulfonation peaks in the FTIR spectra and attributed to the higher polarity of chloroform. The destructive effects of the more intense swelling action on the integrity of the polymer blend were observed in the SEM micrographs. These images showed that chloroform was most disrupted, and dichloroethane most preserved the linearity of the 3D-printed block copolymers throughout the sulfonation reaction. The latter finding was evidence of the milder swelling action of dichloroethane, which may have caused the lower ion exchange capacity of the sample it produced.

By grafting the polymer blends with polystyrene, the interlacing of the SEBS and ABS was stabilized during the sulfonation reaction, which enabled them for ion exchange. Remarkably, this mechanical stability was added to the interpenetrating polymer network without requiring chemical crosslinking. Moreover, the grafting method added additional locations for sulfonation, which increased the ion exchange capabilities of the polymer matrix.

5.2 Future Work

The strategy developed in this research could be fully optimized by graft polymerizing with more iterations of benzoyl peroxide concentration. Further optimization of the grafting effects could be done by varying the degree of polystyrene crosslinking. Moreso, additional steps could be added to the methodology to improve the material's chemistry, stability, and morphology, such as incorporating malic acid to the grafting reaction or commercial ion exchange resins into the polymer blends to create bipolar ion exchange properties.

These findings may be applied to future efforts to improve membrane stability without reducing sulfone domains caused by crosslinking. Specific properties of this method for synthesizing stable ion exchange materials could be applied to fabricate membranes for electrodialysis, pervaporation, and other exciting desalination techniques.

References

Abrams, I. M., & Millar, J. R. (1997). A history of the origin and development of macroporous ion-exchange resins. *Reactive and Functional Polymers*, *35*(1–2), 7–22. https://doi.org/10.1016/S1381-5148(97)00058-8

Alkhudhiri, A., & Hilal, N. (2018). Membrane distillation—Principles, applications, configurations, design, and implementation. *Emerging Technologies for Sustainable Desalination Handbook*, 55–106. https://doi.org/10.1016/B978-0-12-815818-0.00003-5

Banerjee, R., Ray, S. S., & Ghosh, A. K. (2018). Microstructure Development and Its Influence on the Properties of Styrene-Ethylene-Butylene-Styrene/Polystyrene Blends. *Polymers 2018, Vol. 10, Page 400*, *10*(4), 400. https://doi.org/10.3390/POLYM10040400

Barton, B. E., Patton, J. T., Hukkanen, E. J., & Bernius, M. T. (2017). *Two-step sulfonation process for the conversion of polymer fibers to carbon fibers*. Retrieved from https://www.osti.gov/biblio/1408915

Berk, Z., & Berk, Z. (2009). Membrane processes. *Food Process Engineering and Technology*, 233–257. https://doi.org/10.1016/B978-0-12-373660-4.00010-7

Bernardo, P., Drioli, E., & Golemme, G. (2009). Membrane Gas Separation: A Review/State of the Art. *Industrial and Engineering Chemistry Research*, *48*(10), 4638–4663. https://doi.org/10.1021/ie8019032

Chen, G. Q., Wei, K., Hassanvand, A., Freeman, B. D., & Kentish, S. E. (2020). Single and binary ion sorption equilibria of monovalent and divalent ions in commercial ion exchange membranes. *Water Research*, *175*, 115681. https://doi.org/10.1016/J.WATRES.2020.115681

Dahman, Y. (2017). Nanopolymers. *Nanotechnology and Functional Materials for Engineers*,

121–144. https://doi.org/10.1016/B978-0-323-51256-5.00006-X

Dai, J., Wu, S., Han, G., Weinberg, J., Xie, X., Wu, X., … Yang, Q. (2018). Water-energy nexus: A review of methods and tools for macro-assessment. *Applied Energy*, *210*, 393–408. https://doi.org/10.1016/J.APENERGY.2017.08.243

Das, G., Choi, J. H., Nguyen, P. K. T., Kim, D. J., & Yoon, Y. S. (2022). Anion Exchange Membranes for Fuel Cell Application: A Review. *Polymers*, *14*(6). https://doi.org/10.3390/POLYM14061197

de Castro, M. D. L., Capote, F. P., & Ávila, N. S. (2008). Is dialysis alive as a membrane-based separation technique? *TrAC Trends in Analytical Chemistry*, *27*(4), 315–326. https://doi.org/10.1016/J.TRAC.2008.01.015

De Oliveira, A. J. B., De Aguiar, A. P., De Aguiar, M. R. M. P., & De Santa Maria, L. C. (2005). How to maintain the morphology of styrene-divinylbenzene copolymer beads during the sulfonation reaction. *Materials Letters*, *59*(8–9), 1089–1094. https://doi.org/10.1016/j.matlet.2004.12.014

Desrousseaux, C., Cueff, R., Aumeran, C., Garrait, G., Mailhot-Jensen, B., Traoré, O., & Sautou, V. (2015). Fabrication of acrylonitrile-butadiene-styrene nanostructures with anodic alumina oxide templates, characterization and biofilm development test for Staphylococcus epidermidis. *PLoS ONE*, *10*(8). https://doi.org/10.1371/JOURNAL.PONE.0135632

Dharmalingam, S., Kugarajah, V., & Elumalai, V. (2022). Proton exchange membrane for microbial fuel cells. *PEM Fuel Cells: Fundamentals, Advanced Technologies, and Practical Application*, 25–53. https://doi.org/10.1016/B978-0-12-823708-3.00011-0

Garg, M. C. (2019). Renewable Energy-Powered Membrane Technology: Cost Analysis and Energy Consumption. *Current Trends and Future Developments on (Bio-) Membranes:*

Renewable Energy Integrated with Membrane Operations, 85–110. https://doi.org/10.1016/B978-0-12-813545-7.00004-0

Gude, V. G. (2018). Energy Storage for Desalination. *Renewable Energy Powered Desalination Handbook: Application and Thermodynamics*, 377–414. https://doi.org/10.1016/B978-0-12-815244-7.00010-6

Guiga, W., & Lameloise, M. L. (2019). Membrane separation in food processing. *Green Food Processing Techniques: Preservation, Transformation and Extraction*, 245–287. https://doi.org/10.1016/B978-0-12-815353-6.00009-4

Hamiche, A. M., Stambouli, A. B., & Flazi, S. (2016). A review of the water-energy nexus. *Renewable and Sustainable Energy Reviews*, *65*, 319–331. https://doi.org/10.1016/J.RSER.2016.07.020

Helfferich, F. (1922). *Ion-exchange*.

Igor A. Shiklomanov. (1993). World fresh water resources. In Peter H. Gleick (Ed.), *Water in Crisis: A Guide to the World's Fresh Water Resources* (pp. 13–24). New York: Oxford Universtiy Press, Inc.

Iulianelli, A., Clarizia, G., Gugliuzza, A., Ebrasu, D., Bevilacqua, A., Trotta, F., & Basile, A. (2010). Sulfonation of PEEK-WC polymer via chloro-sulfonic acid for potential PEM fuel cell applications. *International Journal of Hydrogen Energy*, *35*(22), 12688–12695. https://doi.org/10.1016/J.IJHYDENE.2010.06.067

Jiang, L. Y. (2016). *Asymmetric Membrane BT - Encyclopedia of Membranes* (E. Drioli & L. Giorno, eds.). https://doi.org/10.1007/978-3-662-44324-8_1762

Jiang, S., & Ladewig, B. P. (2017). High Ion-Exchange Capacity Semihomogeneous Cation Exchange Membranes Prepared via a Novel Polymerization and Sulfonation Approach in

Porous Polypropylene. *ACS Applied Materials and Interfaces*, *9*(44), 38612–38620. https://doi.org/10.1021/acsami.7b13076

Karak, N. (2012). Fundamentals of polymers. *Vegetable Oil-Based Polymers*, 1–30. https://doi.org/10.1533/9780857097149.1

Khalil, A., Ahmed, F. E., & Hilal, N. (2021). The emerging role of 3D printing in water desalination. *Science of the Total Environment*, *790*, 148238. https://doi.org/10.1016/j.scitotenv.2021.148238

Kim, S. (2021). Membranes for Water, Gas and Ion Separation. *Membranes*, *11*(5), 325. https://doi.org/10.3390/MEMBRANES11050325

Kim, Y., & Lawler, D. F. (2011). Selectivity coefficients of cation-exchange membranes: Maximizing consistency and minimizing error amplification. *Separation and Purification Technology*, *81*(3), 357–362. https://doi.org/10.1016/j.seppur.2011.08.002

Kondili, E. (2012). Special wind power applications. *Comprehensive Renewable Energy*, *2*, 725–746. https://doi.org/10.1016/B978-0-08-087872-0.00225-0

Kral, A., Aplin, F., & Maier, H. (2021). Advanced concepts physical chemistry: Electrodes and electrolytes. *Prostheses for the Brain*, 167–208. https://doi.org/10.1016/B978-0-12-818892-7.00014-6

Kumar, P., Bharti, R. P., Kumar, V., & Kundu, P. P. (2018). Polymer Electrolyte Membranes for Microbial Fuel Cells: Part A. Nafion-Based Membranes. *Progress and Recent Trends in Microbial Fuel Cells*, 47–72. https://doi.org/10.1016/B978-0-444-64017-8.00004-X

Kumar Purkait, M., Singh, R., Mondal, P., & Haldar, D. (2020). Pervaporation. *Thermal Induced Membrane Separation Processes*, 99–120. https://doi.org/10.1016/B978-0-12-818801-9.00006-2

Kumar, S., & Jain, S. (2013). History, Introduction, and Kinetics of Ion Exchange Materials. *Journal of Chemistry*, *2013*, 957647. https://doi.org/10.1155/2013/957647

Lee, A., Elam, J. W., & Darling, S. B. (2016). Membrane materials for water purification: design, development, and application. *Environmental Science: Water Research & Technology*, *2*(1), 17–42. https://doi.org/10.1039/C5EW00159E

Loeb, S., & Sourirajan, S. (1964). *Patent No. 3,133,132*. United Sates Patent Office.

Ma, R., Zhao, T., Pu, H., Sun, M., Cui, Y., & Xie, X. (2020). Synthesis of Interpenetrating Polymer Networks Based on Triisocyanate-Terminated and Modified Poly(urethane-imide) with Superior Mechanical Properties. *ACS Omega*, *5*(12), 6911–6918. https://doi.org/10.1021/acsomega.0c00267

Mokrini, A., & Huneault, M. A. (2006). Proton exchange membranes based on PVDF/SEBS blends. *Journal of Power Sources*, *154*(1), 51–58. https://doi.org/10.1016/J.JPOWSOUR.2005.04.021

Müller, F., Ferreira, C. A., Franco, L., Puiggalí, J., Alemán, C., & Armelin, E. (2012). New sulfonated polystyrene and styrene-ethylene/butylene-styrene block copolymers for applications in electrodialysis. *Journal of Physical Chemistry B*, *116*(38), 11767–11779. https://doi.org/10.1021/jp3068415

Nagarale, R. K., Gohil, G. S., Shahi, V. K., & Rangarajan, R. (2005). Preparation and electrochemical characterization of sulfonated polysulfone cation-exchange membranes: Effects of the solvents on the degree of sulfonation. *Journal of Applied Polymer Science*, *96*(6), 2344–2351. https://doi.org/10.1002/app.21630

Orujalipoor, I., Polat, K., Huang, Y. C., İde, S., Şen, M., Jeng, U. S., … Cihangir, N. (2019). Partially sulfonated styrene-(ethylene-butylene)-styrene copolymers: Nanostructures, bio

and electro-active properties. *Materials Chemistry and Physics*, *225*(January 2019), 399–405. https://doi.org/10.1016/j.matchemphys.2018.12.029

Pandey, A. K., Goswami, A., Sen, D., Mazumder, S., & Childs, R. F. (2003). Formation and characterization of highly crosslinked anion-exchange membranes. *Journal of Membrane Science*, *217*(1–2), 117–130. https://doi.org/10.1016/S0376-7388(03)00084-X

Park, H. S., & Hong, C. K. (2021). Anion exchange membrane based on sulfonated poly (Styrene-ethylene-butylene-styrene) copolymers. *Polymers*, *13*(10). https://doi.org/10.3390/polym13101669

Park, M. J., Wang, C., Gonzales, R. R., Phuntsho, S., Matsuyama, H., Drioli, E., & Shon, H. K. (2022). Fabrication of thin film composite polyamide membrane for water purification via inkjet printing of aqueous and solvent inks. *Desalination*, *541*, 116027. https://doi.org/10.1016/J.DESAL.2022.116027

Pretorius, V., Hopkins, B. J., & Schieke, J. D. (1974). Electro-osmosis: A new concept for high-speed liquid chromatography. *Journal of Chromatography A*, *99*(C), 23–30. https://doi.org/10.1016/S0021-9673(00)90842-2

Prifti, H., Parasuraman, A., Winardi, S., Lim, T. M., & Skyllas-Kazacos, M. (2012). Membranes for redox flow battery applications. *Membranes*, *2*(2), 275–306. https://doi.org/10.3390/MEMBRANES2020275

Qian, X., Ostwal, M., Asatekin, A., Geise, G. M., Smith, Z. P., Phillip, W. A., … McCutcheon, J. R. (2022). A critical review and commentary on recent progress of additive manufacturing and its impact on membrane technology. *Journal of Membrane Science*, *645*(October 2021), 120041. https://doi.org/10.1016/j.memsci.2021.120041

Rocha, C. R., Torrado Perez, A. R., Roberson, D. A., Shemelya, C. M., Macdonald, E., &

Wicker, R. B. (2014). Novel ABS-based binary and ternary polymer blends for material extrusion 3D printing. *Journal of Materials Research*, *29*(17), 1859–1866. https://doi.org/10.1557/JMR.2014.158

Salazar Cruz, B., Rivera-Armenta, J., Esquivel De La Garza, A., Morales-Cepeda, A., & Ramos-Galvan, C. (2018). *Study of Dicumyl Peroxide in Crosslinking Process of a SBS- Based Pressure Sensitive Adhesive*.

Sanchez Fernandez, E., Geerdink, P., & Goetheer, E. L. V. (2010). Thermo pervap: The next step in energy efficient pervaporation. *Desalination*, *250*(3), 1053–1055. https://doi.org/10.1016/J.DESAL.2009.09.106

Sarkar, S., SenGupta, A. K., & Prakash, P. (2010). The Donnan Membrane Principle: Opportunities for Sustainable Engineered Processes and Materials. *Environmental Science & Technology*, *44*(4), 1161–1166. https://doi.org/10.1021/es9024029

Schnittker, K., Paso, E., & Gilberto Siqueiros, J. (2016). Methods and polymer compositions for material extrusion 3D printing. *J. Mater. Res*, *29*(17).

Scott, K., & Hughes, R. (1996). Industrial membrane separation technology. In *Industrial membrane separation technology*. London: Blackie Academic & Professional.

Seo, D. W., Lim, Y. D., Lee, S. H., Hossain, M. A., Islam, M. M., Lee, H. C., … Kim, W. G. (2012). Preparation and characterization of block copolymers containing multi-sulfonated unit for proton exchange membrane fuel cell. *Electrochimica Acta*, *86*, 352–359. https://doi.org/10.1016/j.electacta.2012.03.125

Sherazi, T. A. (2016). Styrene-Grafted Film. *Encyclopedia of Membranes*, 1833–1835. https://doi.org/10.1007/978-3-662-44324-8_557

Sirkar, K. K. (2000). Application of membrane technologies in the pharmaceutical industry.

Current Opinion in Drug Discovery & Development, *3*(6), 714—722. Retrieved from http://europepmc.org/abstract/MED/19649899

Soo, A., Ali, S. M., & Shon, H. K. (2021). 3D printing for membrane desalination: Challenges and future prospects. *Desalination*, *520*, 115366. https://doi.org/10.1016/J.DESAL.2021.115366

Stenina, I., Golubenko, D., & Nikonenko, V. (2020). *Selectivity of Transport Processes in Ion-Exchange Membranes : Relationship with the Structure and Methods for Its Improvement*. 25–27.

Strathmann, H. (1981). Membrane separation processes. *Journal of Membrane Science*, *9*(1–2), 121–189. https://doi.org/10.1016/S0376-7388(00)85121-2

Strathmann, H. (1986). *Synthetic Membranes and Their Preparation BT - Synthetic Membranes: Science, Engineering and Applications* (P. M. Bungay, H. K. Lonsdale, & M. N. de Pinho, eds.). https://doi.org/10.1007/978-94-009-4712-2_1

Tavangar, T., Zokaee Ashtiani, F., & Karimi, M. (2020). Morphological and performance evaluation of highly sulfonated polyethersulfone/polyethersulfone membrane for oil/water separation. *Journal of Polymer Research*, *27*(9). https://doi.org/10.1007/s10965-020-02202-5

Tijing, L. D., Dizon, J. R. C., Ibrahim, I., Nisay, A. R. N., Shon, H. K., & Advincula, R. C. (2020). 3D printing for membrane separation, desalination and water treatment. *Applied Materials Today*, *18*(xxxx), 100486. https://doi.org/10.1016/j.apmt.2019.100486

Torrado, A. R., Shemelya, C. M., English, J. D., Lin, Y., Wicker, R. B., & Roberson, D. A. (2015). Characterizing the effect of additives to ABS on the mechanical property anisotropy of specimens fabricated by material extrusion 3D printing. *Additive Manufacturing*, *6*, 16–

29. https://doi.org/10.1016/J.ADDMA.2015.02.001

Torrado Perez, A. R., Roberson, D. A., & Wicker, R. B. (2014). Fracture surface analysis of 3D-printed tensile specimens of novel ABS-based materials. *Journal of Failure Analysis and Prevention*, *14*(3), 343–353. https://doi.org/10.1007/S11668-014-9803-9/FIGURES/14

Vagliasindi, F. G. A., Belgiorno, V., & Napoli, R. M. A. (1998). WATER TREATMENT IN REMOTE AND RURAL AREAS: A CONCEPTUAL SCREENING PROTOCOL FOR APPROPRIATE POU/POE TECHNOLOGIES. *Environmental Engineering and Renewable Energy*, 329–336. https://doi.org/10.1016/B978-0-08-043006-5.50049-5

Wei, H., Li, Y., Wang, S., Tao, G., Wang, T., Cheng, S., … Ding, Y. (2019). Side-chain-type imidazolium-functionalized anion exchange membranes: The effects of additional hydrophobic side chains and their hydrophobicity. *Journal of Membrane Science*, *579*, 219–229. https://doi.org/10.1016/J.MEMSCI.2019.02.058

Wijmans, J. G., & Baker, R. W. (1995). The solution-diffusion model: a review. *Journal of Membrane Science*, *107*(1–2), 1–21. https://doi.org/10.1016/0376-7388(95)00102-I

Xu, T., & Huang, C. (2008). Electrodialysis-based separation technologies: A critical review. *AIChE Journal*, *54*(12), 3147–3159. https://doi.org/https://doi.org/10.1002/aic.11643

Yan, M., Zeng, F., Li, N., Bian, W., Shen, W., & Xie, Z. (2021). Benzene ring crosslinking of a sulfonated polystyrene-grafted SEBS (S-SEBS-g-PSt) membrane by the Friedel-Crafts reaction for superior desalination performance by pervaporation. *Journal of Materials Chemistry A*, *10*(22), 11990–12004. https://doi.org/10.1039/d1ta09700h

Yu, N., Dong, J., Li, H., Wang, T., & Yang, J. (2021). Improving the performance of quaternized SEBS based anion exchange membranes by adjusting the functional group and side chain structure. *European Polymer Journal*, *154*(May).

https://doi.org/10.1016/j.eurpolymj.2021.110528

Zaidi, J. S. M., & Matsuura, T. (Eds.). (2009). *Polymer Membranes for Fuel Cells*. https://doi.org/10.1007/978-0-387-73532-0

Zeman, L. J., & Zydney, A. L. (2017). Microfiltration and ultrafiltration: Principles and applications. In *Microfiltration and Ultrafiltration: Principles and Applications* (pp. 1–618). https://doi.org/10.1201/9780203747223

Zhao, D., Kim, J. F., Ignacz, G., Pogany, P., Lee, Y. M., & Szekely, G. (2019). Bio-Inspired Robust Membranes Nanoengineered from Interpenetrating Polymer Networks of Polybenzimidazole/Polydopamine. *ACS Nano*, *13*(1), 125–133. https://doi.org/10.1021/acsnano.8b04123

Zuo, K., Wang, K., Duchanois, R. M., Fang, Q., Deemer, E. M., Huang, X., … Li, Q. (2021). *Selective membranes in water and wastewater treatment : Role of advanced materials*. *xxx*(xx). https://doi.org/10.1016/j.mattod.2021.06.013

Zuo, K., Wang, K., DuChanois, R. M., Fang, Q., Deemer, E. M., Huang, X., … Li, Q. (2021). Selective membranes in water and wastewater treatment: Role of advanced materials. *Materials Today*, *50*, 516–532. https://doi.org/10.1016/J.MATTOD.2021.06.013

Vita

Avianna Elaine Gallegos conducted her undergraduate studies in Civil Engineering at the University of Texas at El Paso, where she discovered a dual interest in water resource technology and structural design. As an undergraduate student, she worked for the Department of Inland Desalination Systems at UTEP, where she conducted research on electrodialysis and became involved with a water sensor startup as a quality engineer. After graduating with honors, she obtained professional experience in the private sector, working as a staff engineer at a structural engineering firm. During her graduate studies, she continued her collaboration with CIDS and specialized her research in membrane fabrication. She is passionate about using engineering and technological advancements to improve people's lives and hopes to continue her professional career in a way that will contribute to access to clean water and adequate infrastructure in diverse communities. However, she also recognizes that there are limitations to human efforts to improve the world and awaits the moment when Jehovah God will carry out all of his promises to protect our planet and end disease, war, and the unfair distribution of resources, i[o]n exchange for everlasting peace on Earth.

Contact information: aegallegos2@miners.utep.edu